CHAPTER 4

Physical, Structural, Thermal and Electrical Properties of

$x(LiI):(100-x)[60Li_2O:(8B_2O_3+32P_2O_5)]$ glass series

4.1 Introduction to the Glass Series

Fast ionic conductors or electrolytes based on lithium have been extensively studied and utilized in various technologies due to their high ionic conductivity and stability. These properties make them ideal for use in lithium-ion batteries, which are widely used in portable electronic devices such as laptops, smartphones, tablets, in timers and coulometers for accurate timekeeping, in solid-state display (electrochromic) devices, and gas sensors, which detect the presence of specific gases in the environment [1], [2], [3]. They can be used as solid electrolytes in solid-state batteries because they are chemically and electrochemically stable over a wide range. These glasses, which transport lithium ions, can have good electrochemical properties and are being researched as potential electrolytes in "all-solid-state" batteries. These batteries are a type of rechargeable battery that uses a solid-state electrolyte instead of a liquid or gel electrolyte. In an all-solid-state battery, lithium intercalation compounds can be used as the cathode, which is the negative electrode where the lithium ions are stored during charging, and a positive electrode or anode can be made from a variety of materials including lithium metal, lithium-ion insertion compounds, or transition metal oxides [3], [4]. Due to the light weight and highly electropositive nature of lithium metal, electrochemical cells employing lithium ion conducting electrolytes generate high voltage and a specific energy density. It is anticipated that solid electrolytes that conduct lithium ions will play a key role as materials for improved batteries [3]. As a solid electrolyte, one of the most significant features of such glass is that it can change its composition over a wide range. Intriguingly, the mutual interaction of two glass-forming oxides, B_2O_3 and P_2O_5, in the binary system results only in the crystalline compound BPO_4, not glass. The tetrahedra of BO_4, and PO_4, make up its structure. The lithium-ion-conducting borophosphate glasses are a promising candidate for solid-state batteries due to their exceptional ionic conductivity, thermal stability, and electrochemical stability. In the lithium borophosphate glass system, the presence of BO_4 tetrahedra causes the creation of $B-O-P$ bridges, which results in the random branching and compacting of the borophosphate glass network [5]. The structural investigation of the lithium borophosphate glass system with composition $[60Li_2O:(8B_2O_3+32P_2O_5)]$ uncovers the presence of ionic conductivity-enhancing structural groups like BPO_4 and BO_4. In addition, the observed variation in glass transition temperature T_g with composition suggests that there is a correlation between the observed variation in glass transition temperature (T_g) and the composition of the glass. Specifically, this correlation has been linked to structural

modifications in the glass network, particularly with regard to the borate components of the network former [6]. According to Mizerakova, in the lithium borophosphate ternary glass system, the weakening of Coulombic interactions leads to the lowest activation energy and the highest conductivity for lithium ions Li^+ [7]. By reducing the strength of Coulombic interactions, the activation energy required for the movement of lithium ions decreases. This lower activation energy allows for easier movement of the ions within the glass structure, resulting in higher lithium ion conductivity. Katiyar et al.; [2] evaluated lithium cation conductivity since the glass system comprises lithium orthophosphate, diphosphate, and boric acid. According to Dirk Larink [8], the formation of the $B-O-P$ link in the lithium glass system reveals a strong preference for heteroatomic $B-O-P$ linkages over homoatomic $P-O-P$ or $B-O-B$ couplings.

From the literature review, we can say that the transport mechanisms of $Li, Na,$ and Ag ions in the $M_2O-B_2O_3-P_2O_5$; $(Metal\ (M): Li, Na\ and\ Ag)$ glass system have received scant attention to date in terms of ion conductivity and relaxation mechanisms in the metal iodide (MI) doped borophosphate glass system.

Lithium is considered a hard acid because it has a small atomic radius and a high charge density, which means it polarizes electrons strongly. Iodine, on the other hand, is a soft base because it has a large atomic radius and a low charge density, which makes it easy to polarize. When a strong acid like lithium interacts with a weak base like iodine, the resulting bond is often more covalent than ionic. This is because the high charge density of lithium allows it to polarize the electrons of the iodine atom, creating a partially covalent bond. This covalent character can lead to unique properties in the resulting compound, such as enhanced conductivity and relaxation mechanisms. In the modified borophosphate glass system doped with LiI, the softness of the iodine atom may make it easier for Li ions to move through the glass structure, increasing its conductivity. Understanding the conductivity and relaxation mechanism in this system can have important implications for the development of new materials for energy storage and other applications. The structural changes made to the glass network as a result of replacing lithium iodide with $[Li_2O-(B_2O_3-P_2O_5)]$ may be advantageous for the transport of lithium ions. Given that the lithium oxide concentration is maintained at a consistent level throughout the entire series, the variation of LiI in the structural units of glass and their impact on the mobility of lithium ions are directly related to the observed conductivity changes.

In this regard, the current chapter focuses on the glass system with the chemical compound $x(LiI):(100-x)[60Li_2O:(8B_2O_3+32P_2O_5)]$, in which LiI is gradually increased from undoped to weight per cent as $5, 10, 15, 20$ and 25. The composition of each sample is symbolized as $LBPx$, where x represents the $wt.\%$ of lithium iodide salt doped in the sample. In order to get a thorough understanding of the Li^+ ion transport mechanisms involved in the above glass, it is necessary to investigate the relationship between composition, structure, and ionic conductivity, as well as dielectric and modulus studies.

4.2 Experimental

4.2.1 Materials used

Raw materials such as boric acid (H_3BO_3), ammonium dihydrogen phosphate ($ADP-NH_4H_2PO_4$), lithium oxide (Li_2O) and lithium iodide (LiI) were used for preparation of electrolyte materials.

4.2.2 Preparation method

In the present study, composition for the glass samples with x ranging from 0 to 25 $wt.\%$ in the glass series $x(LiI):(100-x)[60Li_2O:(8B_2O_3+32P_2O_5)]$ were prepared using conventional melt quench method. The samples of ionic glass series were prepared initially by taking an adequate quantity of the chemicals and thoroughly mixing them within an agate mortar pestle. Following this, the mixture was kept in the preheated furnace (450℃) for two hours to eliminate NH_3 and CO_2 gas from it. Subsequently, the mixture was allowed to melt at temperatures ranging from $1000℃-1080℃$ for nine hours then being cooled between two pre-cooled copper blocks. For all glass compositions, the created glass specimens were milky transparent. In order to eliminate any thermal stresses that may have been present in the glass as a result of rapid cooling (quenching), I had placed the glass samples in a furnace at a temperature of 150℃ for a duration of half an hour. The Table 4.1 contains a list of the solid electrolyte samples that vary in the concentration of the additive halide-LiI while maintaining the equal ratio of glass former to the modifier.

4.3 Results and discussion

4.3.1 Physical Characterization

Table 4.1 lists the physical specifications of the presented glasses. The density (ρ) increases from $2.46\ g/cc$ to $2.50\ g/cc$ when the LiI salt content increases from 0 to 25 $wt.\%$. This may be related to the rise in iodide ion molecular weight

(126.9045 $g/mole$) in LiI. Confirming the expansion of the glass structure, as depicted in Fig. 4.1(a), the molar volume (V_m) increases from 41.2346 $cc/mole$ to 43.8829 $cc/mole$ when the concentration of lithium salt increases. The structure is also accompanied by a decrease in oxygen packing density (OPD) from 59.1736 mol/l to 42.2038 mol/l while oxygen molar volume (V_O) increases from 16.90 to 23.70 $cc/mole$, meaning volume expansion of the glass upon addition of LiI. However, the modifier oxide does not release as many Li^+as the additive halide as shown in Fig. 4.1(b). The net number of cations released for conduction steadily increases, which may lead to an increase in conductivity, Fig. 4.1(b). Furthermore, the sample code LBP25 has the highest proportion of cations at the Fermi energy level (E_f), as shown by Fig. 4.1(c), which suggests an increase in defect energy states or free charge carriers [1]. As the carrier concentration and mobility of mobile ions affect ionic conductivity, it increases the mobility of the charge carriers with the lowest activation energy for ion migration.

4.3.2 Thermal Characterization

Based on the provided information, it appears that the migration of mobile ions in FIC (Fast Ion Conductor) glasses is attributed to cation dissociation from the rigid glass network [9]. The glass transition temperature (T_g) is a key parameter that can help determine the decoupling index.

The composition of the glasses is directly linked to the glass transition temperature (T_g). In the current system, the addition of LiI (Lithium Iodide) results in a slight decrease in the glass transition temperature from 1063.5 K to 1061.1 K. Table 4.1 shows that as the concentration of LiI increases, the total cation concentration also increases. This increase in cation concentration is expected to enhance ion conductivity.

Furthermore, Fig. 4.1(d) illustrates that the addition of salt (LiI) causes a decrease in the glass transition temperature by up to 25 $wt.\%$. This decrease suggests that charge carriers have been released from the glass, leading to an expansion of the glass structure and increased softness.

Therefore, it can be concluded that the value of the glass transition temperature (T_g) in the present system is composition-dependent, meaning it varies with the composition and concentration of LiI [10].

4.3.3 Structural Characterization

a) X-ray Diffraction study

The X-ray diffraction (XRD) pattern of the LBP series with varying quantities of added halide salt shows (Fig. 4.1(e)) that the samples are completely amorphous and glassy. This is indicated by the broad and dispersed humps visible in the XRD pattern at roughly 30^0 and 50^0. The broadening of these humps with increasing salt concentration suggests that the prepared system becomes increasingly amorphous. Amorphous materials are characterized by a lack of long-range order, which means that the atoms or molecules in the material are not arranged in a regular repeating pattern. This lack of order can lead to increased mobility of the backbone structure, which can enhance ionic conductivity. The results of the XRD study suggest that the addition of halide salt to the LBP series leads to the formation of increasingly amorphous materials with enhanced ionic conductivity. This is a promising finding for the development of new materials for use in energy storage and other applications.

***Table 4.1**: Physical parameters of Lithium borophosphate (LBP) glass electrolyte system.*

Sample code	Network former $(B_2O_3 - P_2O_5)$ (wt.%)	Network modifier (Li_2O) (wt.%)	Additive (LiI) (wt.%)	Density ρ (g/cc)	Molar volume V_m $(cc/mole)$	Oxygen Packing Density OPD $(mole/l)$	Oxygen Molar Volume V_O $(cc/mole)$	cation concentration N_{oxide} x 10^{21} /cc	cation concentration N_{Iodide} x 10^{21} /cc	Total cation concentration N x 10^{21} /cc	N at E_f concentration x $10^{20}/(eV)$ cc
LBP0	40	60	0	2.46	41.23	59.17	16.90	8.76	-	8.76	-
LBP5	38	57	5	2.46	41.89	55.34	18.07	8.20	0.72	8.92	1.60
LBP10	36	54	10	2.47	42.36	51.84	19.29	7.68	1.42	9.10	3.20
LBP15	34	51	15	2.48	42.90	48.34	20.69	7.16	2.11	9.27	4.78
LBP20	32	48	20	2.48	43.50	44.88	22.28	6.65	2.77	9.42	7.31
LBP25	30	45	25	2.50	43.88	42.20	23.69	6.25	3.43	9.68	9.24

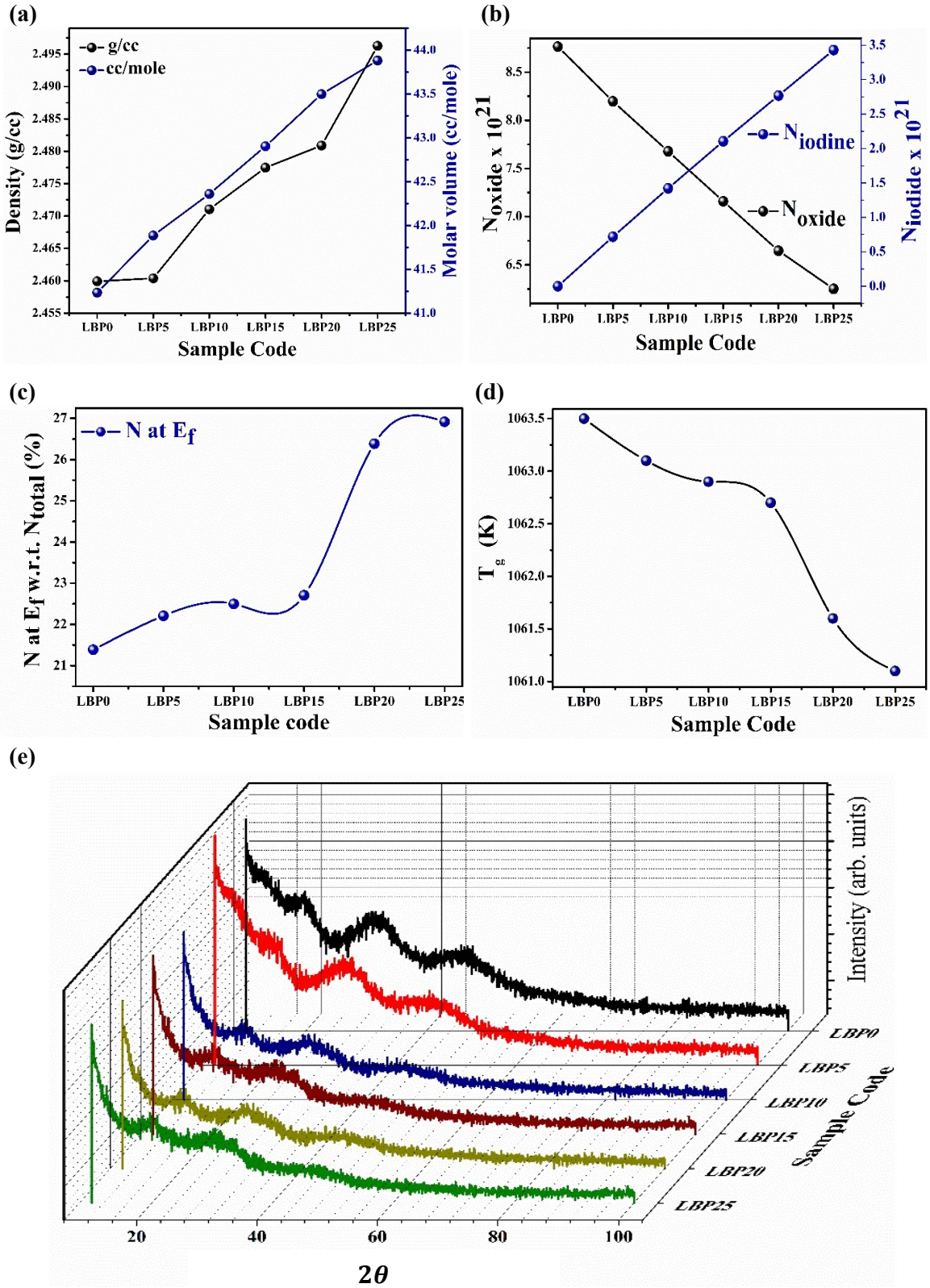

Figure 4.1: *(a) Density and molar volume as a function of LiI additive concentration, (b)Variation of number of charges as a function of modifier oxide and additive halide, (c) Cation concentration at Fermi energy level as a function of glass composition, (d) Glass transition temperature of LBP glass series, and (e) X-ray diffraction pattern for NBP glass series compositions.*

b) Fourier Transform Infrared (FT-IR) Spectroscopy study

Several absorption bands of the LBP glass system are seen in the recorded IR spectra shown in Fig. 4.2. The band positions and their assignments are present in Table 4.2. The absorption bands at the wavenumbers 768 cm^{-1},1103 cm^{-1},1116 cm^{-1},1240 cm^{-1}, 1283 cm^{-1},1334 cm^{-1},1383 cm^{-1}, 1400 cm^{-1}, and 1640 cm^{-1} have been identified to study the present glass system.

The different absorption bands, which are related to the stretching and bending vibrations of the bonds between different atoms or groups of atoms are given below:

- The absorption band at 768 cm^{-1} corresponds to the $B-O-B$ linkage bending in borate network structure [10]–[16].
- The characteristic peak at 1103 cm^{-1} confirms the presence of PO_2 units in the pyro- and meta- phosphate group [16], [17].
- In the lithium borophosphate glass series, $P-O-B$ linkages have a signature peak at 1116 cm^{-1} wave number [18].
- The asymmetric stretching vibration of the $P-O-P$ bond is observed at 1240 cm^{-1} [19], [20], while the asymmetric stretching vibration of $B-O$ bonds of BO_3 unit shows the characteristic peak at 1283 cm^{-1} [21]–[23].
- A characteristic peak near about 1334 cm^{-1} reveals the presence of borate units in pyro- and ortho- borate group [16].

The manifestation of bridging oxygen molecules between triangular borate unit and the tetragonal borate unit are observed and given below.

- The vibration mode at 1383 cm^{-1} is likely due to bridging oxygen molecules between triangular borate units and tetragonal borate units [16].
- The vibration at 1384 cm^{-1}may be attributed to the $P=O$ bond and asymmetric vibration modes of the $P-O-P$ link [11], [24].
- The vibration at 1400 cm^{-1} is associated with the $B-O$ bond and non-bridging oxygen atoms in penta-, ortho-, and pyro- borate groups [16], [18], [25].
- Finally, the peak at 1640 cm^{-1} is related to the asymmetric stretching mode of relaxation vibration in $B-O$ bonds present in trigonal BO_3 units [23].

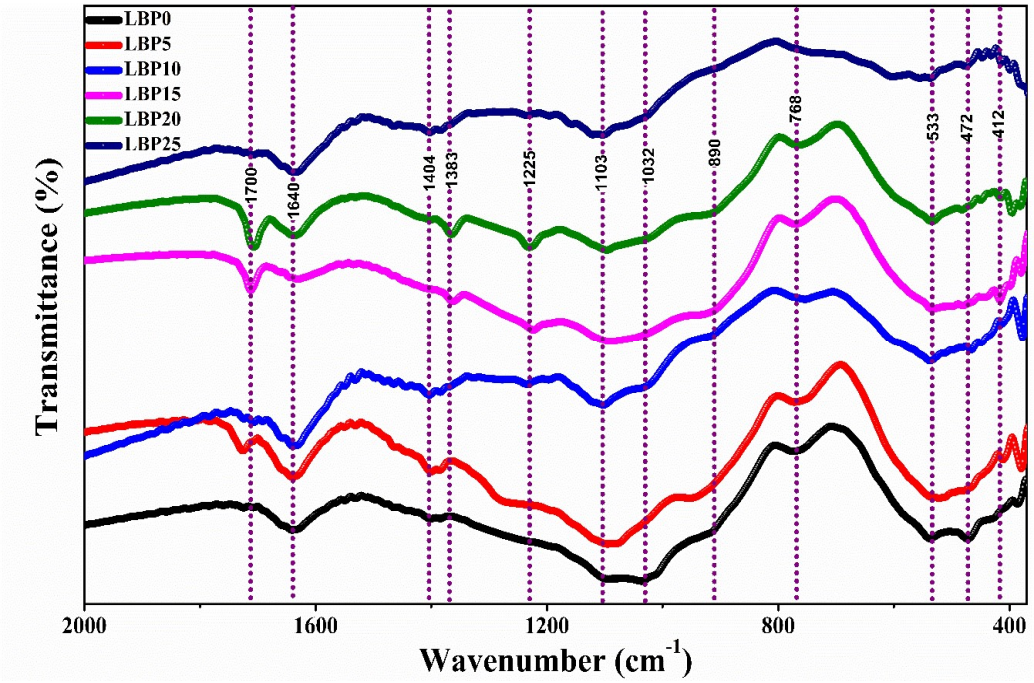

***Figure 4.2**: FTIR absorption spectra of the samples of LBP glass series between* $400\ cm^{-1}$ *to* $2000\ cm^{-1}$ *wave number.*

The addition of LiI to lithium oxide modified boro-phosphate glass can lead to a continuous breakdown of the borate ring structure. This breakdown can result in the polymerization of the borate network. This process can be observed through the shifting of the wave number from $768\ cm^{-1}$ to $780\ cm^{-1}$ for the LBP25 sample. This shift corresponds to the $B-O$ stretching of BO_4 units. Similar observations have been reported by H. Tunt et al; [15], and N.J. Kim [20], and T. Q. Leo et al; [16] have reported that the conversion from BO_3 to BO_4 unit ultimately polymerises the borate network in the glass structure. Form pure LBP sample to LBP25 sample the band at $1103\ cm^{-1}$ goes broadened signifies the formation of tetragonal borate unit.

The absorption band at $1116\ cm^{-1}$ is believed to shift to approximately $1096\ cm^{-1}$ in the lithium oxide modified boro-phosphate glass. This shift may be attributed to the weakening of the double bond character in PO_4 polyhedra. This finding is consistent with the results of previous research work conducted by Kabi and Ghosh [18]. The band at $1240\ cm^{-1}$ appears for LBP10 sample and till $25\ wt.\%\ LiI$ addition in the sample exhibits the broadening of this band can be ascribed to the changes in $P-O-P$ linkage due to formation of cross linking through $P-O-B$ bond formation. The $P-O-P$ linkage is a type of chemical bond that occurs between two phosphate groups. This bond is responsible for the strength and flexibility of the phosphate backbone. The addition of LiI to the LBP series leads to the formation of cross links between the phosphate groups. These

cross links make the backbone more rigid and less flexible. This is reflected in the broadening of the $P-O-P$ band in the IR spectrum. The blur peak at 1383 cm^{-1} is seen in pure LBP glass, which is shifting to the lower wavenumber 1357 cm^{-1} for LBP25 sample, which confirms the elongation of BO_3 units and eventually converting to tetragonal borate group as BO_4 [17], [24].

***Table 4.2**:Band positions and assignments of IR bands of the LBP glass system.*

Wavenumber (Cm^{-1})	Mode of Vibration	Assignment of IR band	Reference
$\sim 755-770$	(ν_s)	• P-O-P in rings of the Bridging Oxygen atoms. Transformation of borate units from BO_3 to BO_4. • B-O-B linkages bending in borate network.	[10], [11], [13], [15], [16], [19], [25]–[28]
$\sim 1100-1150$	(ν_{as}) (ν_s)	• P-O-P of poly-meta chain of (PO_3^-) unit. • NBO from terminal P-O bond and PO_3 unit. • B-O stretching of BO_4units in various borate rings (di-, tri-, tetra-, penta borate groups).	[16], [19], [21], [22], [29]
$\sim 1225-1240$	(ν_{as})	• B-O stretching vibrations of BO_3^- units in penta-, ortho-, pyro- and meta- borate groups. • Metaphosphate $(PO_2)^-$ group. • P=O in PO_4 structural unit with one NBO and change in $P-O-P$ linkage due to formation of $P-O-B$ (cross) link.	[13], [19]–[21], [23], [30]
1283	(ν_{as})	• $B-O$ bonds of BO_3 unit.	[21]–[23]
$\sim 1334-1383$	(ν_s)	• Borate unit in pyro- and ortho- borate group. • BO between BO_3 and BO_4 group. • P=O in NBO atom of phosphate chain PO_2 of NBO in a phosphate chain.	[11], [17], [23], [24], [26]
$\sim 1400-1404$	(ν_{as})*	• Borate triangle unit (BO^-). • B-O bonds associated with NBO in penta-, ortho- and pyro- borate group.	[16], [18], [21], [23], [25]
1627	(ν_{as})	• B–O bond present in trigonal BO_3 units.	[23]

Where, δ_s, ν_s and ν_{as} are the bending, symmetric and asymmetric stretching, and *antisymmetric stretching mode of vibrations, respectively.

The wavenumber at 1400 cm^{-1} for the non-bridging oxygen bonded with $B-O$ link remains unchanged with LiI addition. This suggests that the non-bridging oxygen atoms are not involved in the formation of cross links between the phosphate groups. The wavenumber at 1640 cm^{-1} is observed for LBP0 sample and gradually moves towards 1627 cm^{-1} for 25 $wt.\%$ addition of LiI. This suggests that the trigonal BO_3 units are disappearing and being replaced by tetragonal BO_4 units. The decrease in the wavenumber of the BO_3 unit is due to the elongation of the unit. This elongation is caused by the formation of cross links between the phosphate groups. The gradual increase in

LiI concentration leads to the expansion of the glass structure which is due to the polymerisation of the borate and depolymerisation of phosphate network.

4.3.4 Electrical Characterization / Impedance Spectroscopy

The impedance spectra of the LBP glass series electrolyte samples were studied using the impedance formalism technique. The effect of increasing amounts of LiI on the impedance response of the host glass system, $Li_2O - B_2O_3 - P_2O_5$, is illustrated. The impedance plots for all LBP series compositions over the temperature range of $303\ K$ to $413\ K$, the complex impedance spectra of glasses were measured using the Solartron-1260A for the frequency range of $1\ Hz\ to\ 32\ MHz$.

a) DC conductivity

Fig. 4.3(a-f) depicts the Nyquist plot for all the glass samples and an equivalent circuit for the LBP25 glass at a temperature of $373\ K$ is shown in Fig. 4.3(g). The Nyquist plot given in Fig. 4.3(a-f) shows two semicircles, which is indicative of a kinetically controlled charge transfer mechanism. The diameter of the high-frequency region semicircle gives the bulk (electrolyte) resistance, while the lower-frequency semicircle is caused by the ion diffusion, or "mass transfer resistance," of the electrolyte and the interface between the electrode and the electrolyte [32]. The second semicircle begins to form as the salt (LiI) content in the glass rises and its bulk resistance at high frequencies lowers. This is because the addition of LiI increases the ionic conductivity of the glass, which allows for more ions to participate in the charge transfer process. In the studied frequency range, it is noticed that the thermally stimulated cations contribute to ionic conductivity at high temperatures. This is because the thermal energy at high temperatures allows the cations to overcome the activation energy barrier and move more freely. The results of the Nyquist plot analysis suggest that the addition of LiI to the LBP series leads to the following:

i) Increased ionic conductivity, ii) Reduced bulk resistance, and iii) Increased contribution of thermally stimulated cations to ionic conductivity at high temperatures.

These changes in the ionic conductivity can be expected to affect the properties of the LBP series, such as their electrochemical performance [31]. The dc conductivity is determined by the following Eq. (4.1). Where, σ_{dc} is the dc conductivity, t is the thickness and A is the cross section area of the sample under investigation.

$$\sigma_b = \frac{t}{R_b A} \quad \ldots\ldots (4.1)$$

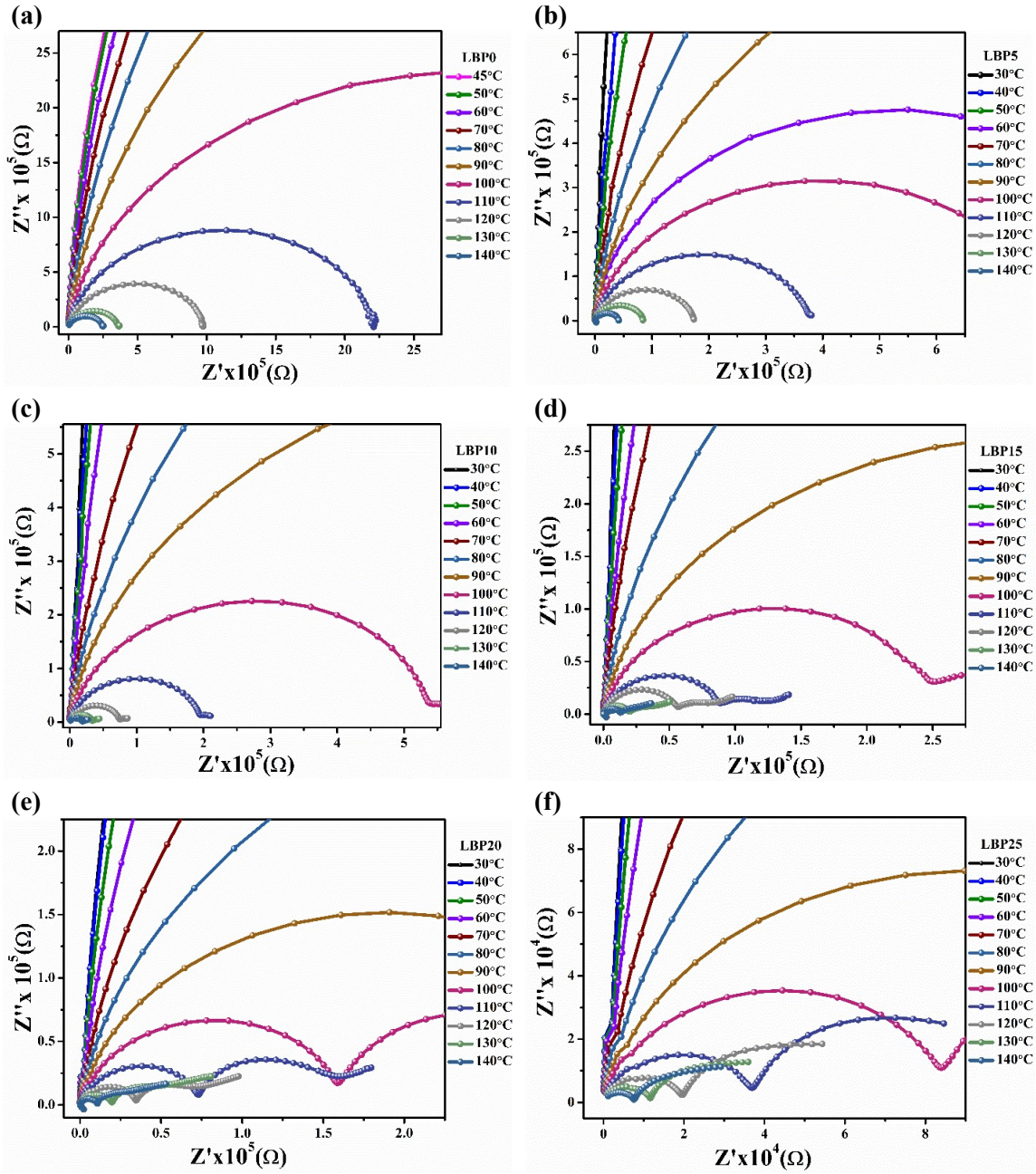

***Figure 4.3**: (a-f) Nyquist plots for LBP series samples for undoped, 5, 10, 15, 20 and 25 (wt.%) of LiI addition in the lithium boro-phosphate glass system respectively.*

An analogous circuit model, as shown in Fig. 4.3(g), was utilized to fit Nyquist plots in order to better understand electrochemical impedance spectroscopy profiles. The fitted model circuit is a helpful tool for understanding the components of the circuit, the time constant, and the dispersion-diffusion processes involved in the Nyquist plot. By analyzing the circuit, various parameters and phenomena can be better understood. The bulk resistance of the specimen (R_b) can be determined by examining the intercept of an arc with the real axis (Z'). This bulk resistance represents the resistance of the overall system or sample being analyzed.

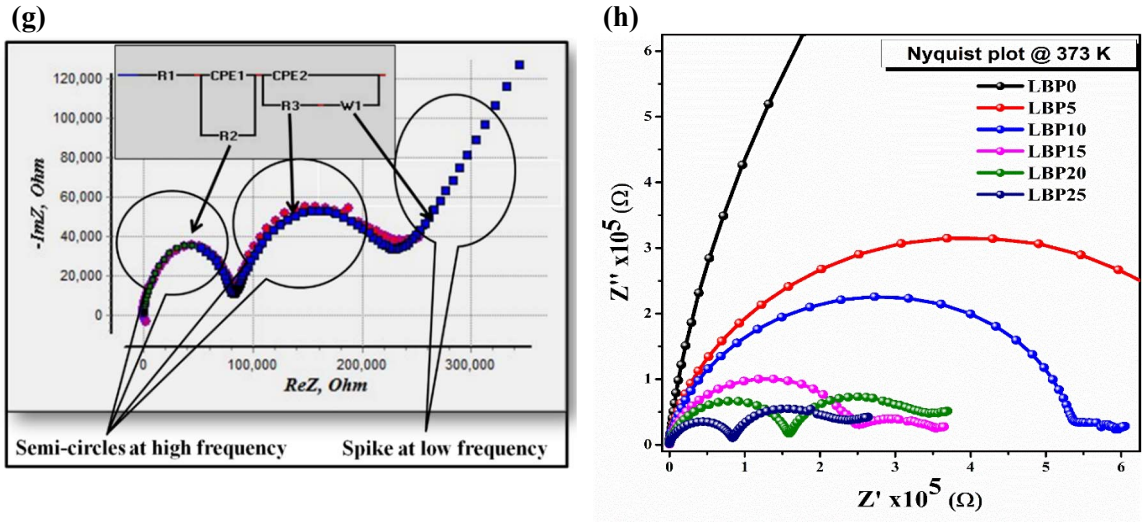

Figure 4.3: *(g) Nyquist plot and the equivalent circuit (inset) for LBP25 sample at* 373 *K (solid line is a guide for eyes), (h) Nyquist plot of glassy electrolytes with* $xLiI$ *in the LBP glass system* ($x = 0$ *to* 25 $wt.\%$) *at* 373 *K temperature.*

When observing a Nyquist plot, the presence of two semicircle arcs on the impedance plot can be explained by a series of two parallel lumped resistances, diffusion coefficients of the ions, constant phase element (CPE) combinations, and a Warburg element. The parallel lumped resistances represent different resistive elements in the system that contribute to the overall impedance. The diffusion coefficients of the ions are associated with the movement of ions within the system, and they influence the transport properties. The constant phase element (CPE) is used to account for non-ideal behavior in the system, such as the presence of capacitance or double-layer effects. It is often used to model the behavior of electrodes or interfaces. The Warburg element is a diffusion-related phenomenon that appears as a linear tail at high frequencies in the Nyquist plot. It represents the impedance associated with diffusion processes occurring within the system. By fitting the experimental data to the model circuit, the parameters of the circuit can be determined, providing valuable insights into the underlying mechanisms and processes occurring in the system under study. The Warburg element is a diffusion element that accounts for the slow diffusion of ions through the electrolyte. The Warburg element is inversely proportional to the square root of frequency. The electrode-electrolyte interface is represented by the CPE element in an equivalent circuit, as shown by inset of Fig. 4.3(g), which stands for the distribution of glass characteristics and is also known as double-layer capacitance effects (CDL). The CPE element is the capacitance that exists between the electrode and the electrolyte. The equivalent circuit model is a powerful tool that can be used to understand the electrochemical impedance spectroscopy (EIS) profiles of materials. The Nyquist plots

of all the series samples show that the arc at high frequency decreases in diameter and tends to migrate towards the origin of the graph, indicating that the impedance value lowers with increasing temperature. Other glass compositions exhibit these temperature-related changes as well. The complex plots show that the semi-circle at the higher frequency is bigger than the arc at the lower frequency. According to the glass compositions at 373 K, the larger and smaller semicircles in Fig. 4.3(h) changed with variations in the corresponding frequency regimes. This is because the larger semicircle is associated with the bulk resistance of the material, while the smaller semicircle is associated with the electrode-electrolyte interface.

Jonscher [34] has shown that glasses are isotropic materials with negligible grain boundary capacitance and resistance. This means that the bulk conductivity of a superionic material is unaffected by the size of its grains. The results of the EIS study suggest that the addition of LiI to the LBP series leads to increased ionic conductivity, reduced bulk resistance, and also increased contribution of thermally stimulated cations to ionic conductivity at high temperatures but isotropic behaviour with negligible grain boundary capacitance and resistance [32]. The centres of the obtained impedance semicircles are below the real axis of the complex impedance plot. The angle between the complex plane origin and the centre of the semicircle explains the degree of asymmetry between the electrode and electrolyte interfaces that may lead to distortion. Fig. 4.4(a) illustrates the variation in ionic conductivities as a function of temperature. It is the $\log \sigma_{dc}$ vs $1000/T$ curve for different LiI concentrations in various system compositions.

$$\sigma_{dc}(T) = \sigma_0 \, exp\left(\frac{-E_a}{kT}\right) \quad \ldots\ldots (4.2)$$

Where σ_{dc} is the ionic conductivity of direct current, T is the temperature in Kelvin, E_a is the activation energy of Li^+ ions, and σ_0 is the pre exponential factor. The activation energy (E_a) necessary for the conduction process is computed using the slope of the dc conductivity curve fitted with the Arrhenius relation, Eq. (4.2), shown in Fig. 4.4(a). The goodness of the linear fit ranges from 0.97532 to 0.99819. Fig. 4.4(b) depicts the dc conductivity and activation energy plot for various salt concentrations.

The addition of LiI to a borate network lowers the activation energy for ion conduction. This is due to the following factors: (i) LiI is a smaller ion than Li_2O, which creates more space for ions to move through the network (ii) LiI is a more polarizable ion than Li_2O, which makes it easier for ions to interact with the network (iii) LiI is a more ionic compound

than Li_2O, which makes it easier for ions to move through the network. The decrease in activation energy leads to an increase in ionic conductivity.

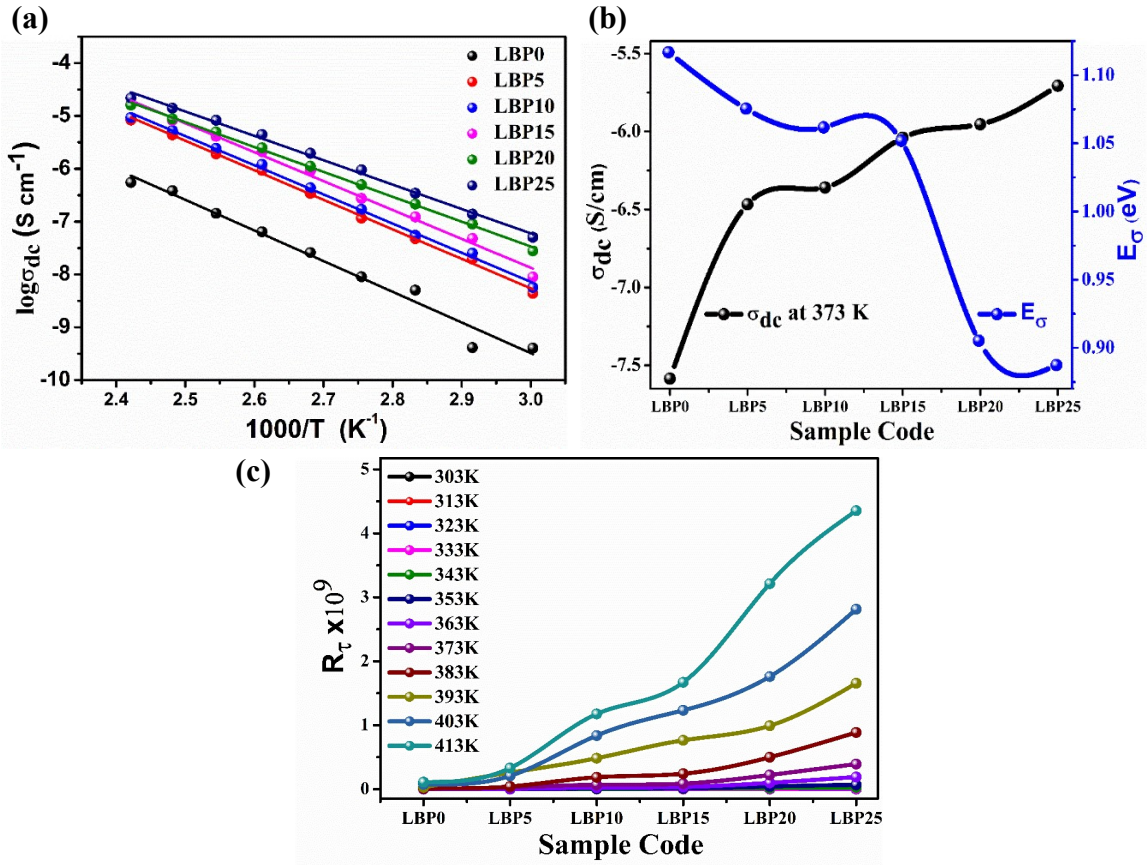

***Figure 4.4**: (a) $\log \sigma_{dc}$ vs. $1000/T$ plot of all glass samples (Sphere indicate the data point and the straight line reflects linear fitting of the trend- a guide to the eyes),(b) Variation of σ_{dc} with activation energy E_σ for LBP glass compositions,(c) Decoupling index (R_τ) at various temperatures for LBP glass series compositions.*

This is because ions can move more easily through the network, which allows for faster charge transport. As seen in Table 4.3, the addition of LiI leads to a decrease in activation energy. This reduction in activation energy implies that less electrostatic binding energy and strain energy are required for the passage of lithium and silver ions. This suggests that the presence of LiI facilitates the movement of ions within the system. Although there is only a small variation in the glass transition temperature (T_g), it is possible that this variation is connected to the rigid structure of the borate network. The addition of LiI may affect the overall structure of the glass, causing slight changes in T_g. As the concentration of LiI increases, the activation energy for the conduction pathway decreases. This activation energy is associated with the trap level beneath the conduction band [33]. Lowering the activation energy indicates that it becomes easier for ions to move through the conduction pathway. The steady decrease in Li^+ ion jump distance, along with the

increase in molar volume (V_m) measurements, supports and confirms the modification of activation energy and conductivity. These observations suggest that the addition of LiI affects the behavior of ions in the system, resulting in changes in activation energy and conductivity.

At various temperatures and/or salt concentrations, the increase in conductivity is linked to the number of charge carriers and/or their mobility that are stimulated thermally. The network former ($B_2O_3 - P_2O_5$) creates tetrahedral sites, into which the salt is introduced at interstitial places and causes the formation of non-bridging oxygen (NBO). The triangular borate units are then changed into tetrahedral borate units by formed NBO.

According to theory, a lower degree of cross-linking the glass network results from the activation energy decreasing and conductivity rising with increased LiI content. In turn, this causes the electrostatic binding energy to drop. The decoupling index $R_\tau(T_g)$ represents the extent to which the motion of conducting ions within a glassy matrix can be separated or dissociated from the viscous motion of the matrix itself at the glass transition temperature (T_g). It is calculated as the ratio of $\tau_s(T_g)/\tau_m(T_g)$, where $\tau_s(T_g)$ represents the average structural relaxation time at T_g, and $\tau_m(T_g)$ represents the average conductivity relaxation time at T_g. The structural relaxation time (τ_s) characterizes the time it takes for the glassy matrix to undergo structural rearrangements or relaxation. This relaxation process is related to the movement of atoms or molecules within the glassy material, which can contribute to its overall viscosity. On the other hand, the conductivity relaxation time (τ_m) refers to the time it takes for the conducting ions to migrate or diffuse within the glassy matrix. This process is associated with the ionic conductivity of the material. By comparing the two relaxation times at T_g, the decoupling index $R_\tau(T_g)$ [37] provides information about the degree to which the motion of the conducting ions is decoupled from the viscous motion of the glassy matrix.

A higher value of R_τ indicates a greater ability to dissociate the motion of the conducting ions from the viscosity of the matrix, suggesting a higher degree of ion mobility or conductivity independent of the structural relaxation of the glassy material.

As seen in Fig. 4.4(c), the decoupling index of the current system, R_τ, given in Table 4.3, rises as temperature and the amount of LiI in the system both rise. It indicates that the conductivity will continue to increase because the motion of the conducting Li^+ ions in the

glassy matrix is becoming decoupled from the viscous motion of the glassy matrix at T_g as the composition and temperature vary.

***Table 4.3**: Various studied physical parameters of the LBP glass system.*

Sample Code	Activation energy E_a (eV)	Calculated at 373 K		Cation $[Li^+]$ concentration $x\ 10^{21}/cc$		
		Conductivity $\sigma_{dc} x\ 10^{-9}$ $(S\ cm^{-1})$	Decoupling index $R_\tau\ x\ 10^6$	$N_1(Li^+)$ Dissociated from Li_2O	$N_2(Li^+)$ Dissociated from LiI	$N_i(Li^+)$ Total no. of $[Li^+]$
LBP0	1.12	26.01	5.19	8.76	-	8.76
LBP5	1.08	341.48	28.86	8.20	0.72	8.92
LBP10	1.06	438.02	68.13	7.68	1.42	9.10
LBP15	1.05	912.74	87.39	7.16	2.11	9.27
LBP20	0.91	1113.67	222.20	6.65	2.77	9.42
LBP25	0.89	1967.11	392.49	6.25	3.43	9.68

b) Frequency dependent conductivity

The ac conductivity of glass samples has been recorded and measured for all LBP glass compositions from $303\ K$ to $413\ K$ temperature and $1\ Hz$ to $32\ MHz$ frequency range. Fig. 4.5(a-f) and 4.6(a) refer to figures related to the ac conductivity. The ac conductivity depends on both temperature and composition: The study shows that the electrical conductivity of the material(s) under investigation is influenced by two factors: temperature and composition. This means that changes in temperature and the composition of the material(s) have an impact on the conductivity. It is obvious that the frequency-dependent conductivity, denoted as $(\sigma'_{(\omega)})$. This refers to the conductivity of the material(s) at different frequencies. The symbol ω represents the angular frequency. When increasing the LiI content within the studied range of frequencies, the frequency-dependent conductivity $(\sigma'_{(\omega)})$ shows consistent behavior. This behavior is observed at a specific frequency range associated with the relaxation phenomenon. The study findings are consistent with similar results obtained by Meenakshi Dult et al;[33] in borosilicate glasses, and in lithium bismuth borate glasses by Mahmoud et al; [34]. This suggests that the observed behavior of ac conductivity with respect to temperature and composition is not unique to the material investigated in this particular study, but has also been observed in other types of glasses. Fig. 4.5 depicts the frequency-dependent conductivity of LBP glass electrolyte samples at various temperatures.

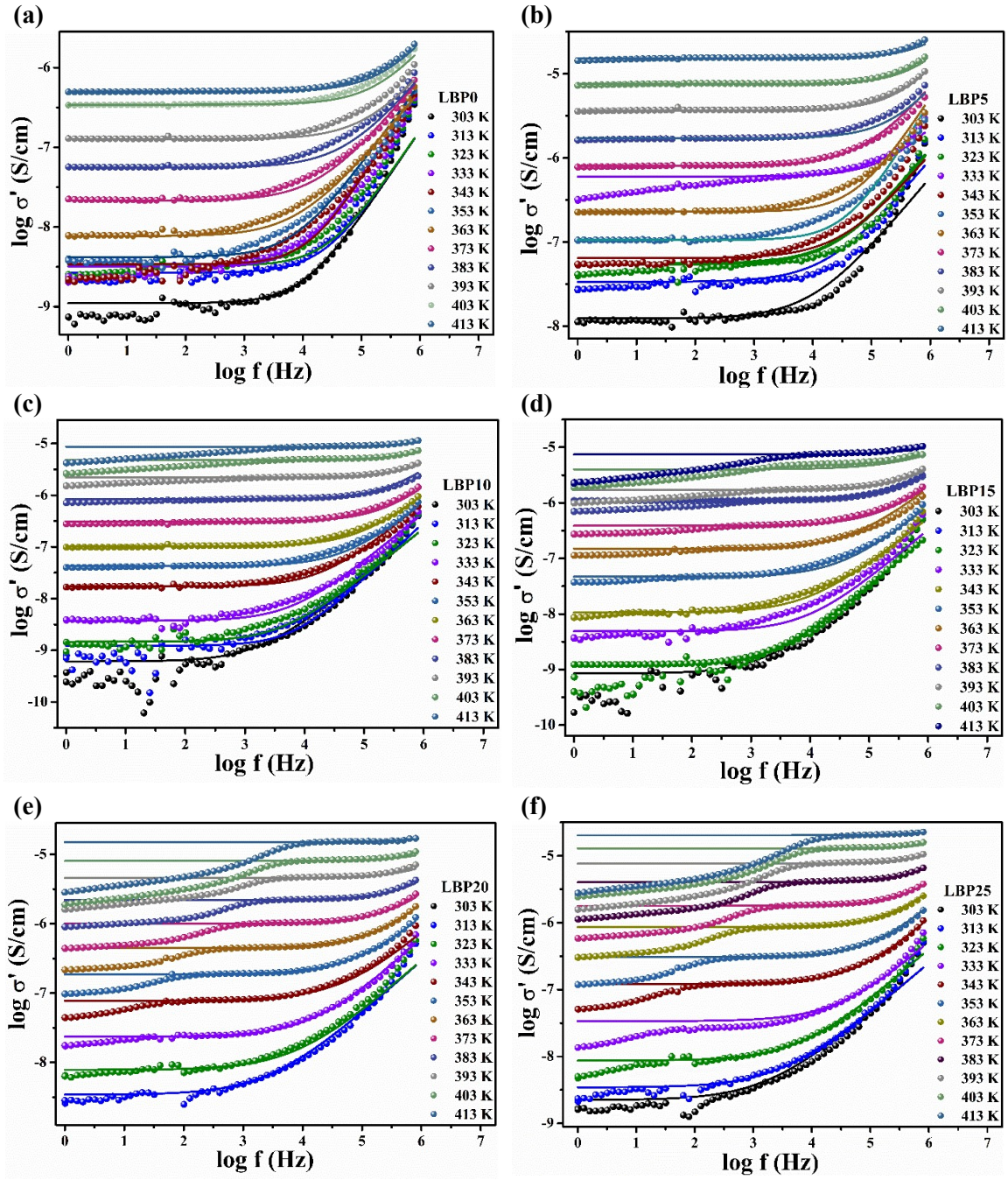

***Figure 4.5**: (a-f) The plots of σ'vs frequency at various temperatures for $x = 0, 5, 10, 15, 20$ and $25\ wt.\%$ of LiI in the borophosphate glass, respectively (straight line represents the JPL fitting and guide to eyes).*

In Fig. 4.5(a-f) and 4.6(a), the frequency-dependent conductivity (σ'_ω) displays two key regions: plateau and dispersion. At low frequencies, there is a plateau region where the conductivity remains constant and is independent of frequency. This behavior arises due to the random distribution of charge carriers through activated hopping, which means the charge carriers move by hopping from one localized state to another. Within the plateau region, the conductivity is frequency-independent. This means that regardless of the

frequency of the applied electric field, the conductivity of material remains the same. The conductivity value observed in this region is referred to as the dc conductivity (σ_{dc}). At higher frequencies, beyond the plateau region, a dispersion region is observed. In this region, the conductivity (denoted as $\sigma'_{(\omega)}$) continues to increase as the frequency (ω) increases. This indicates a frequency dependency of conductivity. The temperature has an effect on the frequency range spread within the plateau region. As the temperature increases, the dispersion region becomes narrower, meaning that the range of frequencies over which the conductivity deviates from the plateau value decreases. As the frequency increases further into the dispersion region, the conductivity spectra become more dispersed. This dispersion means that the conductivity values at different frequencies become more spread out, indicating a broader range of conductivity values at higher frequencies. At very high frequencies, the conductivity spectra may appear to merge or converge. This suggests that at extremely high frequencies, the conductivity becomes less dependent on the frequency and may approach a limiting value.

The samples from LBP15 (Fig. 4.5(d)) begin to exhibit a second dip in the lower frequency range as a result of charge accumulation due to polarization. As the temperature rises, the conductivity transition shifts to a greater frequency as the mobile ions acquire thermal energy and overcome the barrier potential more easily. The frequency-dependent ac conductivity is usually formulated and fitted by Jonscher's universal power law [10], [35], as shown in Fig. 4.5(a-f) and 4.6(a).

$$\sigma_{ac} = \sigma_{dc} + A(\omega)^n \quad \ldots\ldots (4.3)$$

where A is the characteristic parameter, ω is the radial frequency, and n is the temperature- and frequency-dependent power exponent (usually denoted as $n(T)$). The values of σ_{dc}, A, and n are derived from the experimentally determined frequency-dependent conductivity ($\sigma'_{(\omega)}$) at various temperatures. The observed increase in conductivity in the current glass samples can be attributed to two factors: the increase in the thermally activated total number of cations and/or their drift velocity as the temperature rises. Research conducted by M. Gabr et al., P. V. Rao et al., and other research teams in various glass systems [38]–[40] have reported similar findings.

Table 4.3 shows that the total number of cations $N_i(Li^+)$ in the current glass system, specifically Li^+ ions, increases from $8.764\ x\ 10^{21}\ /cc$ for LBP0 sample to LBP25 sample with $9.682\ x\ 10^{21}\ /cc$. This increase in the number of cations contributes to a higher concentration of charge carriers available for conduction.

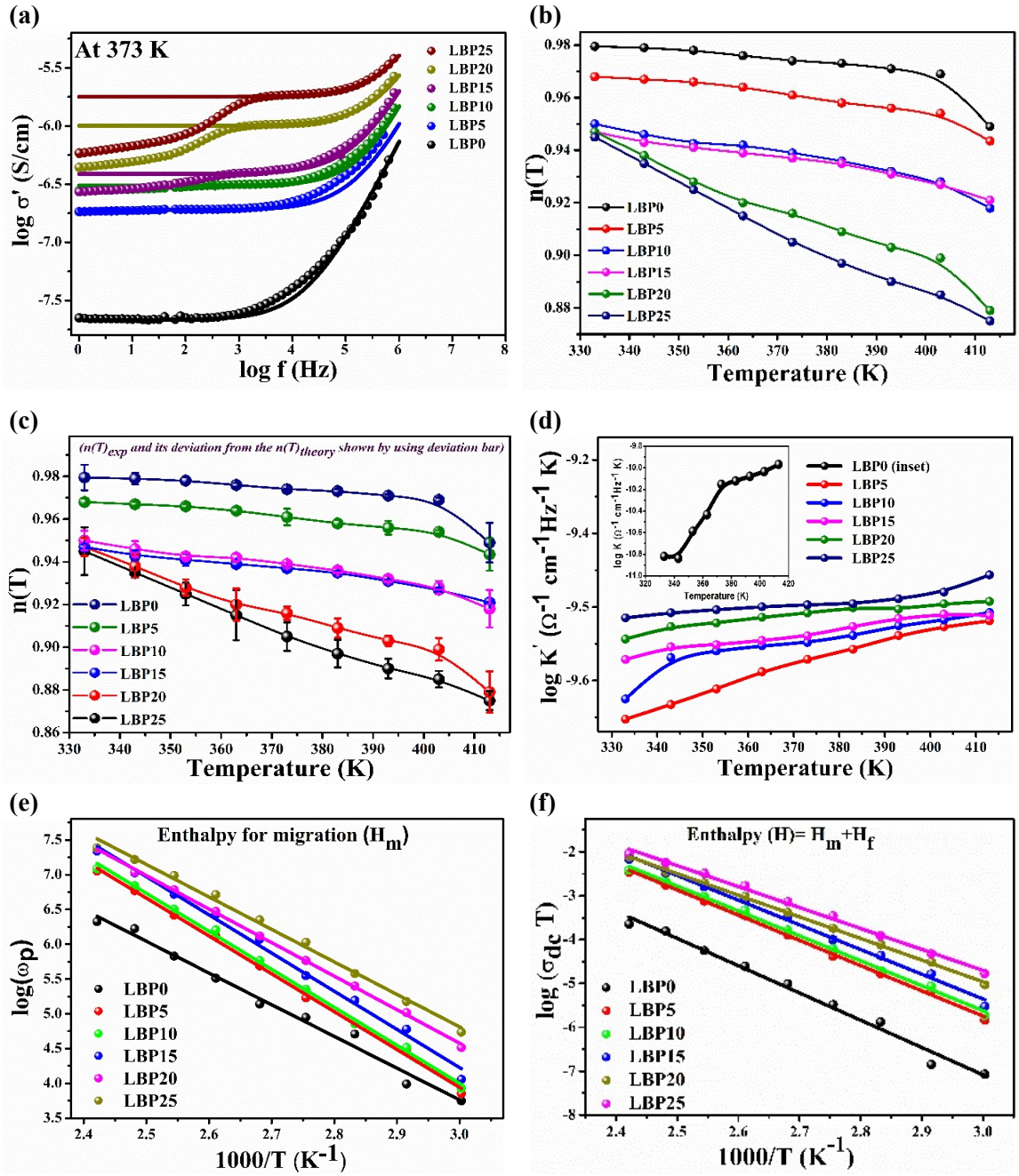

***Figure 4.6**: (a-f) For all the glass samples of LBP series (a) Variation of ac conductivity (straight line shows JPL fitting) as a function of log frequency at 373 K, (b) Frequency exponent (n) as a function of temperature, (c) Theoretical and experimentally obtained value of power exponent, (d) Mobile ion concentration K' as a function of temperature, (e) Enthalpy for migration (H_f) estimated using hopping frequency vs inverse of temperature trend, (f) Total enthalpy (H) derived from the slope of linear fitted $\log(\sigma_{dc}\,T)$ vs. inverse of temperature plot (solid lines are the guide to the eyes).*

The conductivity at room temperature also varies accordingly, ranging from $10^{-8}\,S/cm$ for the LBP0 sample to $10^{-6}\,S/cm$ for the LBP25 sample. The conductivity values demonstrate an increase in the ability of the glass samples to conduct electric current, which is consistent with the higher number of cations available for conduction. Therefore, the

increase in conductivity in the current glass samples can be attributed to the rise in the thermally activated total number of cations (specifically Li^+ ions) and/or their drift velocity with increasing temperature.

- **Conductivity scaling**

The Summerfield and Roling scaling are mathematical expressions that describe the relationship between the ac (alternating current) conductivity and the dc (direct current) conductivity of a material. These scaling laws provide a way to relate the conductivity at different frequencies and temperatures using a universal function. The mathematical explanation of the Summerfield scaling in its most elementary version.

$$\frac{\sigma'}{\sigma_0} = F\left(\frac{f}{\sigma_0 T}\, x\right) \ldots\ldots \quad (Summerfield\ canonical\ scaling)$$

Where, f is the frequency, σ_0 is the conductivity at a given temperature, T is the absolute temperature, x is concentration (of dopant) factor. At $\omega = \omega_p$, the ac conductivity can be equated with dc conductivity as $\sigma'(\omega) = 2\sigma_{dc}$.

The Roling scaling assumes that the charge carriers in the material are constant with temperature and that the plasma frequency (ω_p) is thermally activated with the same quanta of energy as the product of dc conductivity (σ_{dc}) and temperature (T). It relates the ac conductivity (σ') to the dc conductivity (σ_{dc}) through the universal function F, which depends on the frequency (f), dc conductivity (σ_{dc}), and temperature (T).

$$\frac{\sigma'}{\sigma_0} = F\left(\frac{f}{\sigma_{dc} T}\right) \ldots\ldots \quad (Roling\ canonical\ scaling)$$

The universal function F, which is indifferent to changes in temperature and chemical composition, describes the ion dynamics in this equation. The most significant benefit of such scaling law is that it uses the quantities that are already available as scaling parameters, allowing for a simpler mathematical description of the relationship between ac and dc conductivities in materials. The universal function F encapsulates the underlying physics and provides a way to characterize ion dynamics across. As illustrated in Fig. 4.6(g-l), the ac conductivity (σ') data is scaled by dc conductivity (σ_{dc}), while the parameters $\sigma_{dc}T$ or say ω_p (Summerfield) [36], and $\sigma_{dc}T_x$ (Roling) [37], [38], are respectively utilised to normalise the frequency axis.

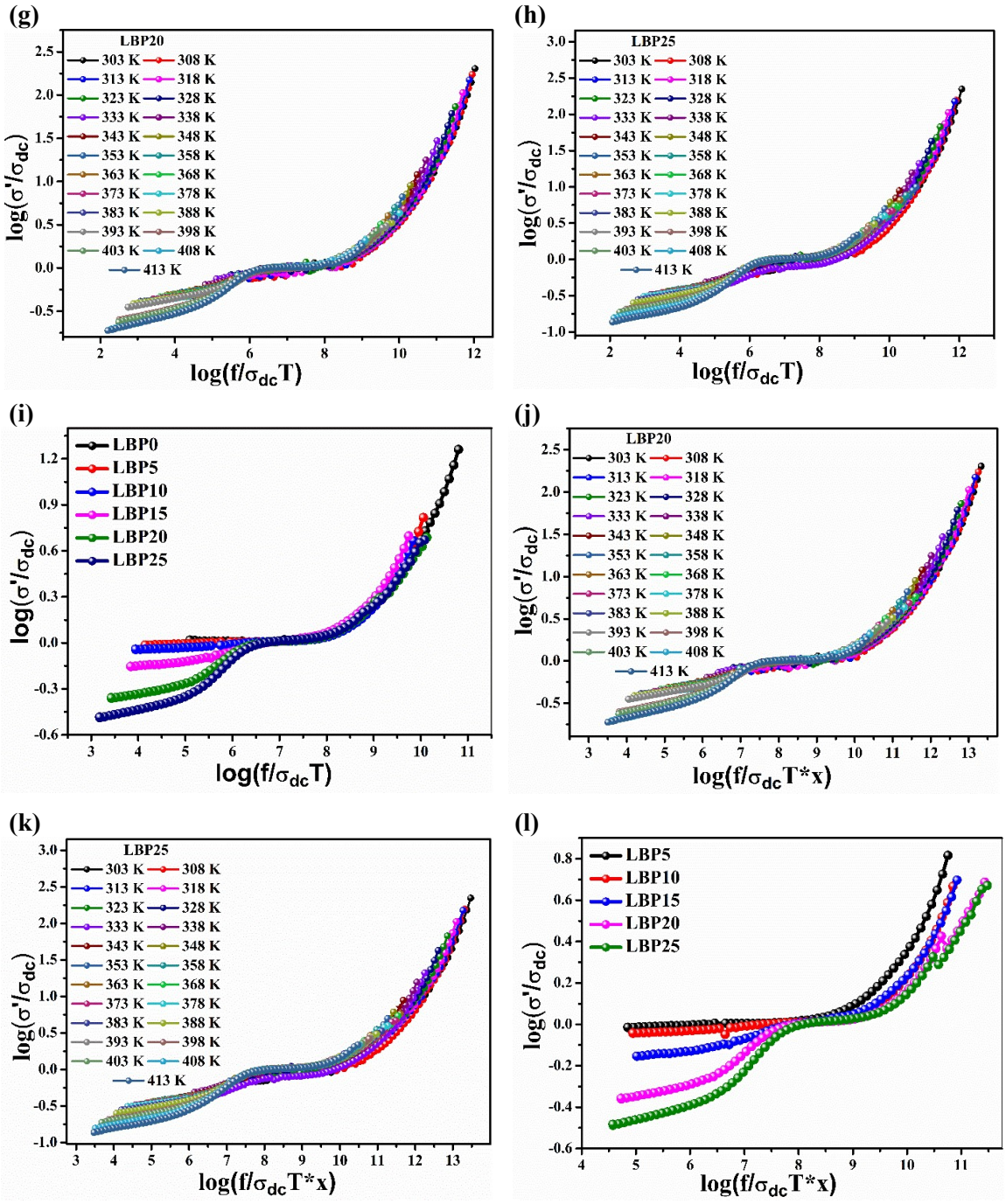

***Figure 4.6**: Plots of normalized conductivity spectra with frequency using (g-i) Summerfield formalism, (j-l) Roling model formalism; respectively for LBP20, LBP25 at various temperatures and for all the samples at 373 K temperature.*

The ac conductivity spectra, depicted in Fig. 4.6(g-h and j-k), exhibit a nearly perfect merging into a single master curve for different temperatures. This behavior indicates the presence of a phenomenon called Time-Temperature Superposition (TTS), suggesting that there is a temperature-independent conduction mechanism at play. This phenomenon was first described by Sidebottom [44] and is also known as canonical scaling. However, it is important to note that the merging of spectra into a master curve is not observed at very low

frequencies near the polarization region, as shown in Fig. 4.6(g-h and j-k). In the present investigated system, the lack of merging in this frequency range can be attributed to changes in the concentration of Li^+ ions and slightly varied ion transport behavior within the glass at a specific temperature. Fig. 4.6(i and l) shows the scaling of ac spectra with frequency scaling using the Summerfield and Roling formulations, respectively, for different concentrations of LiI at a temperature of 373 K. This analysis demonstrates the impact of the mobile ion concentration (Li^+) and modifications in the glass structure. The statement suggests that while the electrical conductivity spectra for different LiI concentrations do not show a complete overlap, the scaling formulations put forth by Roling and Summerfield, though different, provide reasonable agreement with the experimental data for the system being studied. This indicates that these scaling formulations capture the effects of mobile ion concentration and modifications in the glass structure to a certain extent.

Based on the description provided, it appears that Fig. 4.6(d) shows the concentration of mobile ions (represented as K') as a function of the quantity of LiI in the LBP25 specimen. The graph shows an upward trend, indicating that as the amount of LiI increases, the concentration of mobile ions also increases. This upward trend continues until it reaches its maximum level in the LBP25 specimen. According to the findings of Roling, significant variation in ion concentration have a considerable impact on the relaxation of ions. In the context of the study or experiment being described, it suggests that the variations in mobile ion concentration, specifically the concentration of K' affect the relaxation behavior of ions. The statement also mentions that the phenomenon of scaling with respect to composition is commonly observed in glasses that exhibit significant fluctuations in mobile ion concentration. In other words, when there are substantial changes in the composition of the glass, there tends to be considerable variation in the concentration of mobile ions. This variation is known to be dependent on changes in the glass composition.

Eq. (4.4) and (4.5) are used to calculate the density of states, $N(E_f)$, and the average distance between two cations, R', in the context of thermally induced electron hopping at the Fermi level (E_f) and cation concentration and its transport phenomenon in a system [31], [33].

$$N(E_f) = \frac{3}{4\pi R'^3 E_a} \quad \ldots\ldots(4.4), and\ R' = \sqrt[3]{(1/N)} \quad \ldots\ldots(4.5)$$

These equations are derived to understand the transport phenomena and cation behavior. In Eq. (4.4), $N(E_f)$ represents the number of energy states available at the Fermi level. It is

determined by two factors: the volume of the system ($4\pi R'^3$), and the activation energy (E_a). The equation suggests that as the volume between cations decreases (smaller R'), and the activation energy increases, the number of energy states at the Fermi level increases. Eq. (4.5) describes the relationship between the average distance between two cations, R', and the number of cations, N_i. The term $\sqrt[3]{(1/N)}$ represents the inverse of the cube root of the cation density. As the cation concentration increases (larger N_i), the average distance between cations (R') decreases. From Table 4.4, it is observed that the value of $N(E_f)$ increases from $1.60\,x10^{20}eV^{-1}cm^{-3}$ to $9.24\,x10^{20}eV^{-1}cm^{-3}$ in the glass network of LBP5 to LBP25 samples. This indicates that the number of defect energy states or free charge carriers has increased. Moreover, the average distance between lithium ions (R'_{LiI}) becomes smaller over time, implying easier movement or migration of ions. These observations suggest changes in the cation concentration and transport phenomena in the examined samples. The frequency power exponent ($n(T)$) has been incorporated into the discussion in order to comprehend the interaction between the ion and the network. A smaller value of $n(T)$ represents a higher degree of network modification [10], [33], [34]. The conduction mechanism in the system under study is determined by analyzing the power exponent, $n(T)$. The obtained values of $n(T)$ are used to understand the conduction mechanism [39].

In this particular system, the analysis of $n(T)$ supports the hopping mechanism for conductivity. The behavior of $n(T)$ for all the samples at different temperatures is depicted in Fig. 4.6(b). It is mentioned that there is a drop in the value of $n(T)$ within the temperature range being studied. This decrease in $n(T)$ is believed to be connected to the Correlated Barrier Hopping (CBH) process of conduction [33], [34], which is a type of hopping mechanism where the charge carriers are correlated, meaning that they are more likely to jump to sites that are close to each other. The decrease in $n(T)$ with increasing temperature is due to the fact that the thermal energy of the charge carriers increases. As the thermal energy increases, the charge carriers are more likely to have enough energy to jump over the barriers that separate the localized sites. This results in an increase in the conductivity of the material. Fig. 4.6(c) illustrates the experimentally measured values of $n(T)$ (represented by spheres) and the theoretically anticipated values (represented by a line) as both decreasing with temperature. The error bar in the figure indicates the difference between the observed value and the expected value of $n(T)$.

Eq. (4.6) represents the mathematical expression for the fraction of total mobile charge carriers (n') in a conduction process that occurs through a defect mechanism.

$$n' = Ne^{\left(\frac{-G_f}{kT}\right)} = Ne^{\left(\frac{S_f}{k}\right)}.Ne^{\left(\frac{-H_f}{kT}\right)} \quad \ldots\ldots(4.6)$$

The above equation is an exponential function that involves both the formation energy and enthalpy of the defect, as well as the temperature. The negative sign in the exponent indicates an inverse relationship between the fraction of mobile charge carriers and the energy/temperature factors. A higher formation energy or enthalpy, or lower temperature would result in a lower fraction of mobile charge carriers. Conversely, a lower formation energy or enthalpy, or higher temperature, would lead to a higher fraction of mobile charge carriers. The mobile ion concentration factor K' mentioned earlier influences the behavior of conductivity, shown in Fig. 4.6(d), as suggested by the rising trend of charge carrier concentration from the LBP5 to the LBP25 sample. The values of K' are likely affected by factors such as hopping frequency, temperature, and dc conductivity, as mentioned. It's worth noting that while Eq. (4.6) provides a mathematical expression to describe the fraction of mobile charge carriers (n') in a defect mechanism, the specific values of the formation energy, enthalpy, and other parameters would depend on the material system and the defects involved.

$$\omega_p = \omega_0 e^{\left(\frac{S_m}{k}\right)}.e^{\left(\frac{-H_m}{kT}\right)} \quad \ldots\ldots(4.7)$$

$$\sigma_{dc} = \frac{NZ^2e^2d^2\gamma\omega_0}{kT} e^{\left(\frac{S_f+S_m}{k}\right)} e^{\left(-\frac{H_f+H_m}{kT}\right)} \quad \ldots\ldots(4.8)$$

According to Eq. (4.6), the parameters associated with the dissociation of cations from their original sites adjacent to the charge compensation center are N, the total charge carriers, entropy (S_f), enthalpy (H_f), and free energy (G_f). The cross over (hopping) frequency (ω_p) is given by Eq. (4.7), and the dc conductivity is given in the form of a dissociation process by Eq. (4.8). In these equations, a frequency of attempts is denoted by ω_0; ion migration related parameter including entropy (S_m) and enthalpy (H_m); the geometric and correlation constant is denoted by γ, the jump distance is given as d. The analysis of conductivity versus the inverse of temperature plot in relation to the conduction mechanism in ionic glasses has been done. According to Jain and Mundy [46], this plot can be used to explain the behavior of conductivity in such materials. The total enthalpy in the system consists of two main components: the free energy (H_f) and the migration energy (H_m), which describes the dissociation of cations from their initial positions near the charge

compensating center [36]. To further analyze the system, logarithmic plots of the hopping frequency ($\log \omega_p$) and the product of dc conductivity and temperature ($\log (\sigma_{dc} T)$) versus $1/T$ are created using Eq. (4.7) and (4.8) respectively. The plots correspond to these functions are displayed in Fig. 4.6 (e and f). In the current system, the value of H_m is determined by performing linear fitting of the logarithm of hopping frequency against the inverse of temperature graph shown in Fig. 4.6(e). The range of goodness of fit for this linear regression is between 0.9854 and 0.9990. Similarly, to determine the value of enthalpy with respect to the reciprocal of temperature, a linear fit is performed on the logarithm of $(\sigma_{dc} T)$ versus $1/T$ plot shown in Fig. 4.6(f). The goodness of fit for this linear regression ranges from 0.98564 to 0.99888.

Table 4.4: *Experimentally obtained data for LBP glass series.*

Sample Code	$N(E_f)\ x10^{20}\ eV/cc$	Measured value at 373 K			R'_{LiI} (Å)	Enthalpy (eV)		
		$\omega_p\ (x10^6\ Hz)$	$U_M\ (eV)$	$R_{min}(1MHz)$ (Å)		Migration H_m	Free energy H_f	$H = H_m + H_f$
LBP0	-	0.14	7.42	59.22	-	0.88	0.32	1.20
LBP5	1.60	0.49	4.95	79.11	11.16	1.05	0.06	1.11
LBP10	3.20	0.58	3.16	1.27	8.89	1.05	0.04	1.09
LBP15	4.78	1.18	3.06	98.05	7.80	1.06	0.03	1.09
LBP20	7.31	1.32	2.30	1.46	7.12	0.93	0.02	0.95
LBP25	9.24	2.25	2.03	1.52	6.63	0.90	0.02	0.92

For the temperature of 373 K, the values of ω_p are displayed in Table 4.4, which shows that the hopping frequency shifts from 0.14 MHz to 2.25 MHz with the addition of lithium salt. Using the slopes of linearly fitted plots, the values of the enthalpy for migration H_m and the total enthalpy ($H = H_f + H_m$) are computed and displayed in Table 4.4 for LBP series samples. According to this, the value of H_f is found to be greater than zero in case of current system under investigation. It indicates that at a particular time, the total number of charge carriers exceeds the total number of mobile charge carriers. Hence, it is obvious that the conductivity of the current glass system increases with LiI content due to both the concentration and mobility of charge carriers [33].

Ion transport model

According to several conduction mechanism models, the variation of $n(T)$ with temperature in the applied ac field varies in different ways. Various models describe the behavior of the exponent $n(T)$ in different conduction mechanisms as a function of temperature. Each mechanism exhibits a distinct pattern of variation, indicating the different physical processes at play in each case.

1. Overlapping Large Polaron Tunneling (OLPT) conduction process [47]:
   - As temperature rises, the exponent $n(T)$ initially drops.
   - It reaches a minimum value at a particular temperature.
   - After reaching the minimum, it starts increasing again.
2. Quantum Mechanical Tunneling (QMT) conduction mechanism [48]:
   - The exponent $n(T)$ is approximately equal to 0.8.
   - It either slightly increases with rising temperature or remains temperature independent.
3. Non-Overlapping Small Polaron Tunneling (NSPT) conduction process [49]:
   - The exponent $n(T)$ rises with temperature.
4. Correlated Barrier Hopping (CBH) conduction process [36], [49]– [53]:
   - The value of $n(T)$ follows a decreasing trend as temperature rises.

According to the CBH model, the empirical expression for the power exponent $(n(T))$ is given in Eq. 4.9.

$$n(T) = 1 - \frac{6kT}{U_M + kT\ln(\omega\tau_0)} \quad \ldots\ldots (4.9)$$

If the maximum barrier height at a given temperature is given as $U_M \gg kT$ and $\omega\tau_0 \sim 1$, where τ_0 is the downward jump time constant. When the field is applied, the modified values of the frequency dependent power exponent and hopping distance, $R_{min}(\text{Å})$, can be expressed as Eq. 4.10.

$$n(T) = 1 - \frac{6kT}{U_M} \quad \ldots\ldots (4.10)$$

The calculated values of maximum barrier height (U_M), effective barrier height (U_H), and frequency-dependent hopping distance (R_{min}) are also given in Table 4.4.

$$R_{min} = \frac{e^2}{\pi\varepsilon'\varepsilon_0 U_M} \quad \ldots\ldots (4.11)$$

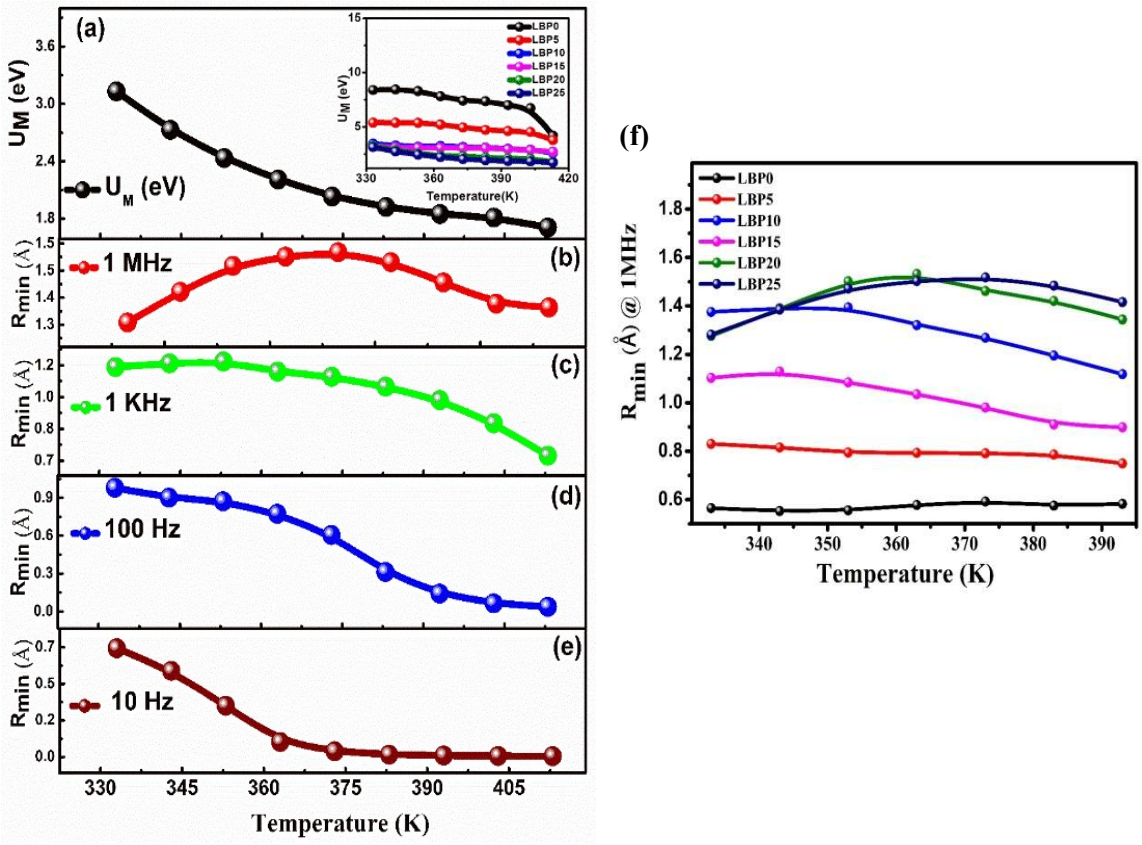

Figure 4.7: *(a) At various temperature, the max barrier height* (U_M) *for LBP25 glass composition. (inset:* U_M *as a function of temperature for all the glass compositions), (b-e) The minimum hopping distance* (R_{min}) *vs Temperature at various frequencies, (f) The variation of minimum hopping distance* (R_{min}) *for all glass composition at different temperatures at 1 MHz frequency.*

In this case, the Eq. (4.12) describes how the Coulomb wells of neighboring sites affect the effective barrier height (U_H) when a charge carrier (e) moves through hopping between these sites. The equation is expressed as:

$$U_H = U_M - \frac{e^2}{4\pi\varepsilon'\varepsilon_0 R} \quad \ldots\ldots (4.12)$$

where, e denotes the charge carrier, ε' the dielectric constant of a substance, and ε_0 the permittivity of open space. Eq. 4.12 suggests that the effective barrier height (U_H) is reduced from U_M (the energy needed to remove the electron entirely from the site) due to the overlapping of the Coulomb wells of neighboring sites separated by the distance $R_{(Li-Li)}$. The extent of reduction depends on the distance between the sites (R) and the properties of the medium through which the charge carrier moves (characterized by the dielectric constant ε'). The Coulomb interaction between the charge carriers in the wells affects the energy required for the carrier to traverse the barrier. Additionally, the R-finite separation

between two neighboring hopping sites (Å), and the characteristic relaxation time (τ_0) having a typical value of $10^{-13}\ sec$ is comparable to the vibrational period of an atom. According to the CBH model, the AC conductivity can be calculated as follows:

$$\sigma_{ac} = \frac{\pi^3}{12} N^2 \varepsilon' \varepsilon_0 \omega R_\omega^6 \quad \ldots\ldots (4.13)$$

where, N is the number of sites in a pair and R_ω is the hopping distance at a certain frequency ($\omega = 2\pi f$), and it can be expressed as Eq. (4.14).

$$R_\omega = \frac{2e^2}{\pi \varepsilon' \varepsilon_0 \{U_M + kT\ ln(\omega \tau_0)\}} \quad \ldots\ldots (4.14)$$

It is evident from inset of Fig.4.7 (a), that the value of maximum barrier height (U_M) declines with temperature and the amount of LiI in the lithium boro-phosphate glass skeleton, while Fig. 4.7(a-e) shows that R_{min} decreases with temperature at various frequencies. For all the glass compositions presented in Fig. 4.7(f), R_{min} likewise exhibits the temperature-decreasing trend, Eq. (4.11), which is suggestive of the CBH process. As a result, it may be assumed that the CBH model of conduction mechanism for ion transport holds true for all glass samples of LBP glass series.

c) Dielectric Study

The investigation of frequency-dependent dielectric relaxation contributes to comprehend the ion transport mechanism in ion-conducting materials. In the present glass system, a study of the dielectric parameters as a function of frequency and temperature has been conducted. The complex dielectric function ε^*, which is related to complex impedance and conductivity values, can be expressed as Eq. (4.15).

$$\varepsilon^* = \frac{1}{i\omega C_0 Z^*} = \frac{\sigma^*(\omega)}{i\omega\varepsilon_0} = \varepsilon'(\omega) - i\varepsilon''(\omega) \ldots\ldots (4.15)$$

According to this definition, the dielectric constant, denoted as ε', represents the real part of permittivity and is related to the static permittivity ($\varepsilon' = \varepsilon_s$). It arises from the accumulation of charge carriers (ions) and the alignment of dipoles induced by an electric field. Essentially, it describes how much the material can store electric energy when subjected to an electric field. On the other hand, the dielectric loss, denoted as ε'', represents the imaginary part of permittivity. It accounts for the energy dissipation in the system due to both dipole alignment and ion mobility. When an electrical field is applied to the material, the motion of mobile ions can be described using the dielectric loss.

However, due to their high inertia, mobile ions respond slowly to rapidly changing electric fields. As a result, a loss peak is observed at high frequencies in the dielectric loss spectrum. This peak indicates the energy dissipated in the system during the alignment of dipoles and the mobility of ions. The loss tangent $(\tan\delta)$ is a ratio that expresses the energy dissipation $(\varepsilon^{"})$ to the energy stored (ε') in the system. It is often defined at the peak of field-induced polarization and provides valuable information about the efficiency of energy transfer and dissipation in the material [40]. For various samples of the lithium borophosphate glass system, the temperature-dependent dielectric constant and dielectric loss graphs at various frequencies are shown in Fig. 4.8(a-c) and (d-f) respectively. It has been found that the ε′ and ε" steadily rise as temperature increases. It is well known that the behavior of the dielectric parameters ε′ and ε" is with respect to frequency. It states that at lower frequencies, both ε′ and ε" have higher values, but as the frequency increases, they follow a downward trend. At a specific frequency called the "dispersion frequency," the values of ε′ and ε" become almost constant, regardless of the frequency. This behavior can be observed marginally for the LBP25 sample in Fig. 4.8(c) for ε′ and Fig. 4.8(f) for ε". The dielectric parameters ε′ and ε" provide information about the dielectric properties of a material. In this case, the values of ε′ and ε" show a particular trend in the spectra.

They are higher in the low-frequency range and gradually decrease in the mid-frequency dispersive region. Fig. 4.8(a-f) depicts the rapid increase in the dielectric constant (ε') and dielectric loss $(\varepsilon")$ at a low frequency $(\sim 1\ kHz)$. The saturation plateau is eventually seen at the high frequency and is seen in Fig. 4.9(a-b) [41], [42] at an arbitrary temperature. According to figures, the high-frequency saturation plateau is clearly visible for glass compositions with $x = 0$ to 25 $wt\%$ of LiI, but lower-frequency plateau $(\boldsymbol{\varepsilon_s})$ appears to have combined with that due to polarization effects and cannot be distinguished.

It is the result of a phenomenon known as the "electron polarization effect," occurs when mobile cations are obstructed at the interface between a glass sample and an electrode. This obstruction prevents the transfer of mobile ions into external circuits through metallic electrodes [58]. As a result of this obstruction, lithium mobile ions begin to accumulate near the electrodes, leading to bulk polarization of the sample. The accumulation of these ions causes a polarization effect throughout the material. In high-frequency regions, specifically above the dispersion frequency, the applied electric field quickly reverses.

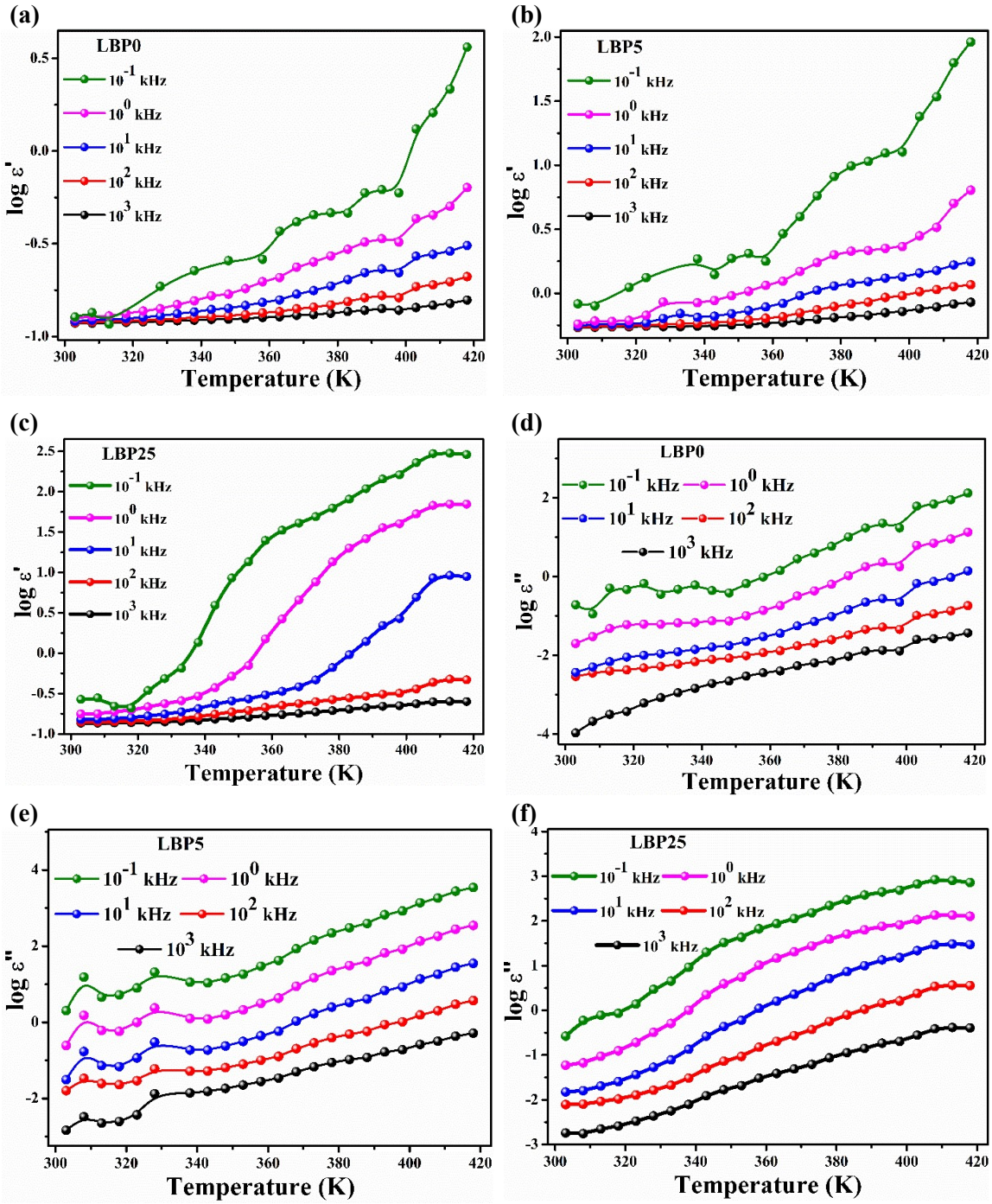

***Figure 4.8**: Frequency dependent dielectric parameters for various LBP glass samples, (a-c) Dielectric constant (ε′) as a function of temperature, (d-f) Dielectric loss (ε") as a function of temperature.*

During this reversal, the ions do not move significantly or hop between positions due to the high energy barrier. As a result, polarization is lost on the side opposite to the high energy barrier.

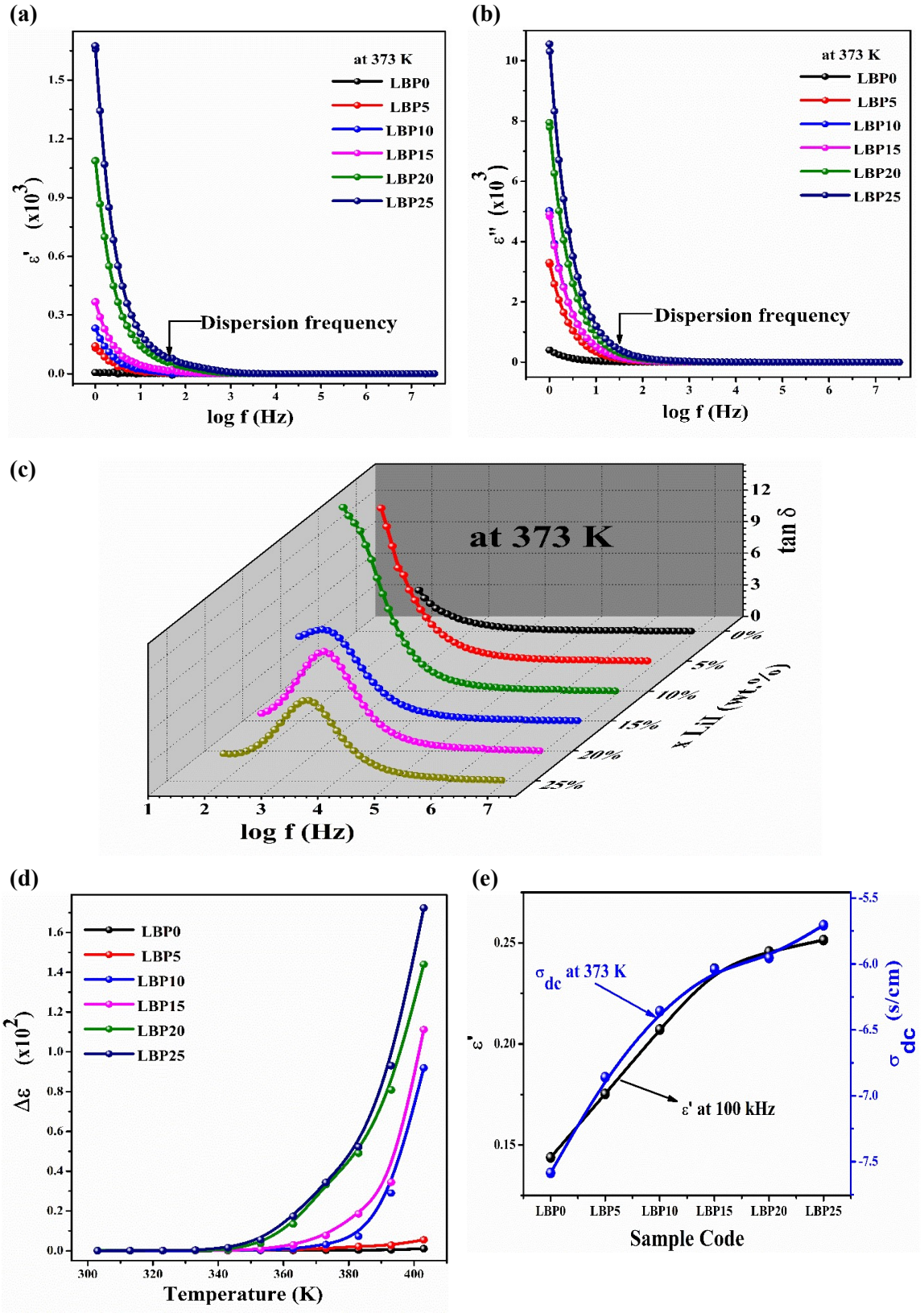

***Figure 4.9**:(a) Dielectric constant, (b) dielectric loss, (c) tan δ as a function of frequency at 373 K temperature, (d) Dielectric relaxation strength (Δε) variation with temperature, and (e) trend line for dielectric constant at 100 kHz frequency and conductivity at 373 K temperature, for all the glass compositions.*

Additionally, the value of the real part of the dielectric constant (ε') saturates or reaches a maximum due to the accumulation of mobile ions near the electrodes and the inability of the ions to respond effectively to the quickly reversing electric field. Many other research groups have noticed and reported similar characteristics of dielectric dispersion [41], [42].

Various observations and relationships related to the addition of LiI to a lithium borophosphate glass system can be described. Fig. 4.9(c) shows the peak of field-induced polarization. By analyzing the shifts in the peak frequency of the loss spectra, it is possible to distinguish between different samples. The addition of LiI affects the peak frequency, causing it to shift from the lower frequency side to the higher frequency side. The frequency-dependent variation in dielectric permittivity ($\Delta\varepsilon = \varepsilon_s - \varepsilon_\infty$) provides insights into dielectric polarization. Fig. 4.9(d) illustrates the temperature versus "dielectric relaxation strength" ($\Delta\varepsilon$) plot, which represents multiple relaxation processes. It indicates that both temperature (thermal activation) and LiI concentration contribute to a progressive increase in the dielectric strength. Fig. 4.9(e) presents the relationship between conductivity and the dielectric constant of the glass system under investigation. The graph clearly demonstrates that the addition of LiI enhances both the frequency-dependent dielectric constant and the temperature-dependent conductivity.

The dielectric constant, loss and loss tangent as a function of frequency are also evident from the Fig. 4.10(a-f). The discussion highlights that the increase in the peak loss value with the increase in LiI salt concentration is due to the migration of LiI ions into the glass matrix. This migration leads to conduction losses and dipolar relaxation losses, collectively known as ion migration losses, which contribute to the dielectric loss. However, it is mentioned that in the studied frequency range, no loss peak is observed.

This implies that the frequency range under consideration may not be suitable for observing the loss peak or that the loss peak occurs at a higher frequency range. Further investigations may be required to explore the frequency dependence of the dielectric loss and to determine the frequency range at which the loss peak occurs.

Overall, the discussion provides valuable insights into the effect of LiI salt concentration on the dielectric loss spectra of LBP glass and highlights the importance of understanding the underlying mechanisms of ion migration losses in such systems.

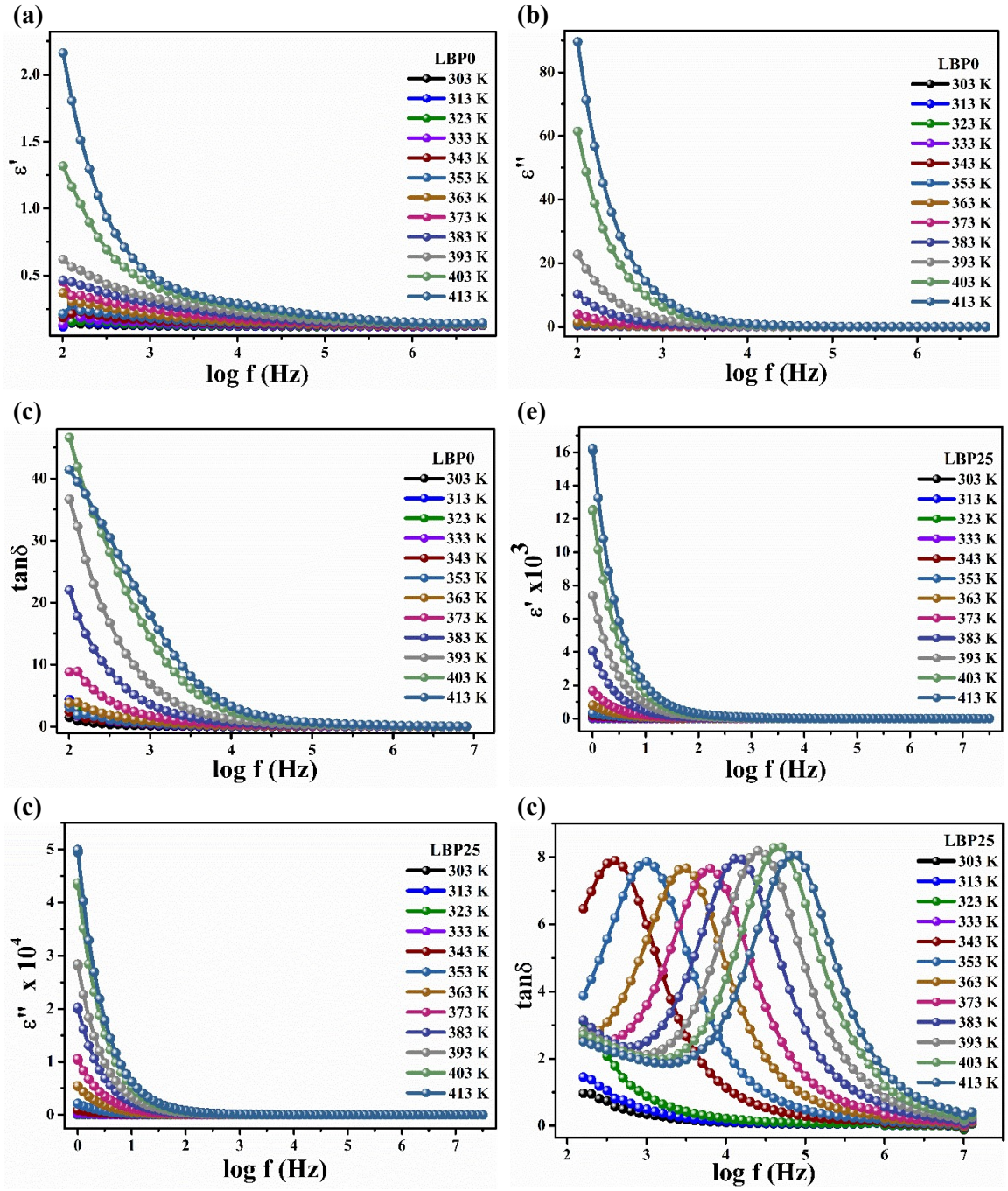

***Figure 4.10**:(a, d) dielectric constant, (b, e) dielectric loss, and (c, f) loss tangent, as a function of frequency for LBP0 and LBP25 glass samples respectively.*

Fig. 4.10(c and f) exhibits the tan δ plot wherein, the rise in temperature causes the shift in peak frequency towards higher frequency regime and explains the dielectric relaxation phenomenon for the glass samples. The frequency dependent dielectric study reveals that the strength of the dielectric relaxation increases progressively with both temperature and the addition of *LiI* in the studied LBP glass system. The presence of *LiI* in the glass matrix leads to an enhancement in both the dielectric constant and conductivity parameters. This suggests that the addition of *LiI* improves the overall electrical properties of the glass. The

migration of Li^+ ions into the glass matrix contributes to an increase in the dielectric loss as the salt content rises. This indicates that the presence of LiI facilitates the movement of charge carriers, resulting in higher energy dissipation through the dielectric relaxation process. Among the investigated glassy electrolyte samples, the $25\,wt.\%$ LiI-added sample exhibited the most significant improvements in conductivity and dielectric properties. This suggests that the optimal composition for enhanced electrical performance in the LBP glass system is achieved with the addition of $25\,wt.\%$ LiI.

Overall, the inclusion of LiI in the glass composition leads to improved conductivity and dielectric properties, as demonstrated by the frequency dependent dielectric study in the studied LBP glass system.

d) Electric Modulus Study

The modulus formalism has the advantage of excluding frequency-dependent dielectric conductivity data caused by electrode polarization at contact or interfaces, Maxwell-Wagner effects, or a high dielectric constant. The "Modulus Formalism" introduced by Macedo et al. [59] is a novel approach to analyze relaxation spectra and overcome the challenges associated with distinguishing between relaxation behavior and polarization effects when separating the dc conductivity from total conductivities.

In traditional analysis techniques, such as frequency-dependent conductivity ($\sigma'_{(\omega)}$), it can be difficult to separate relaxation behavior and polarization effects due to the large experimental error. However, the modulus formalism offers a solution by transforming the continuously varying frequency-dependent conductivity ($\sigma'_{(\omega)}$) into a representation where a peak is observed in the modulus $M'_{(\omega)}$. The modulus formalism allows for a clearer distinction between relaxation behavior and polarization effects by focusing on the peak in the modulus representation. This peak provides valuable information about the relaxation processes occurring in the material under investigation. By using the modulus formalism, researchers can enhance their understanding of relaxation phenomena and obtain more accurate and reliable results in the analysis of relaxation spectra. This formalism provides a valuable tool for characterizing the behavior of materials and can be applied in various fields, such as solid-state physics, materials science, and electrochemistry. The data is more apparent when it is presented using modulus scaling approach (discussed under the next heading).

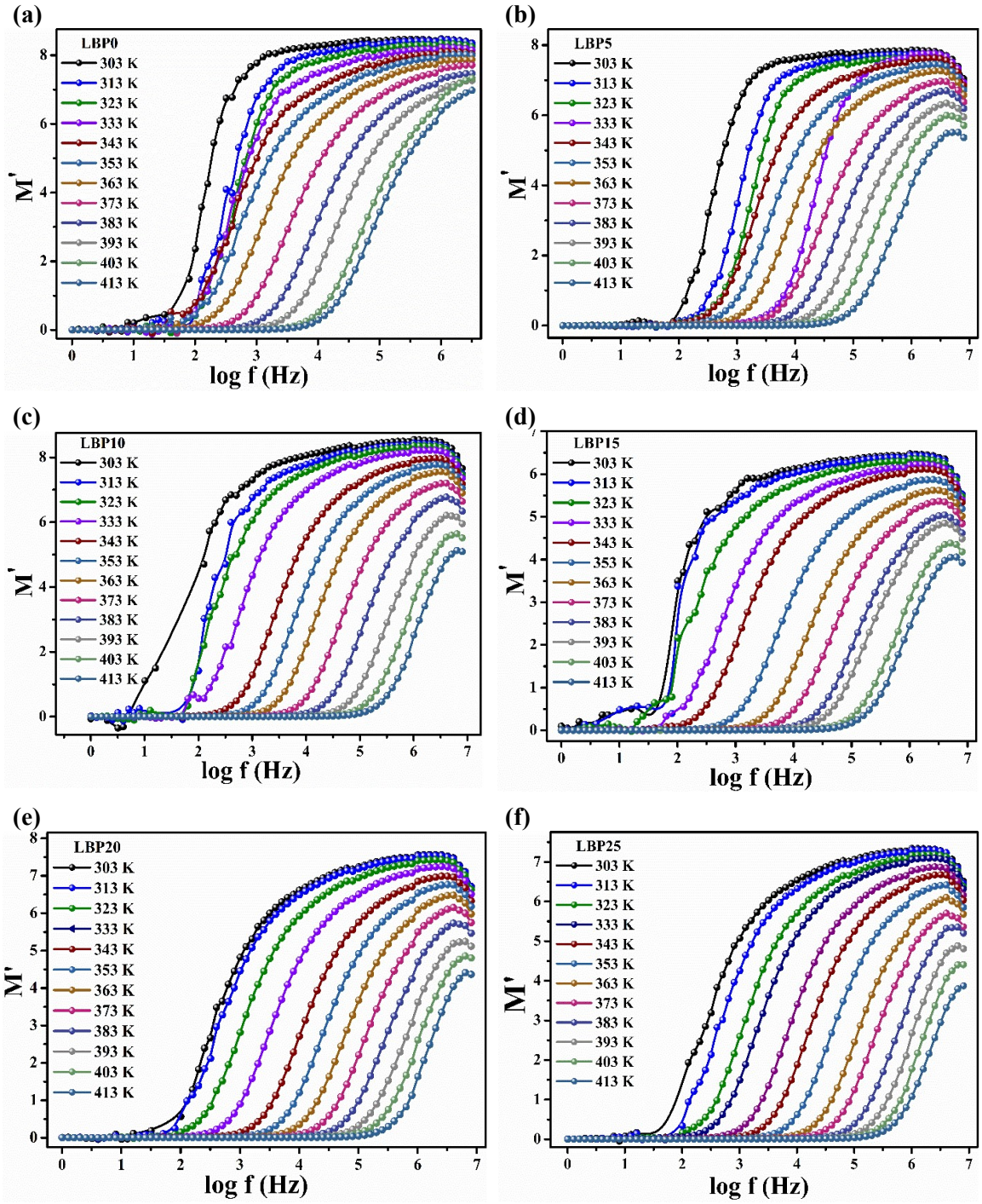

***Figure 4.11**:(a-f) The plot of $M'_{(\omega)}$ as a function of frequency for xLiI addition in lithium borophosphate glass system, where $x = 0,\ 5, 10, 15, 20, 25\ wt.\%$ respectively.*

Fig. 4.11(a) depicts the real component of the modulus spectrum, $M'_{(\omega)}$, for a pure LBP glass sample at various temperatures. Similarly, all other samples exhibit identical behavior when $x = 5\ to\ 25\ (wt.\%)\ LiI$ salt is added to lithium borophosphate glass, as shown in Fig. 4.11(b–f).

The figure illustrates that: M' tends towards zero at lower frequencies: This suggests that the real part of the complex modulus, M', decreases as the frequency decreases. It indicates that electrode polarization has a minimal impact on the overall behavior of the system at lower frequencies. Impact of electrode polarization on M^* is insignificant. The complex modulus, M^*, is the combination of both the real part (M') and the imaginary part (M''). The statement implies that the effect of electrode polarization on the overall magnitude of M' is negligible. Dispersion refers to the frequency dependence response of a material. In this case, the dispersion is mainly due to conductivity relaxation. This means that the electrical conductivity of the material changes as a function of frequency. As the frequency increases, the real part of the complex modulus, M', reaches a maximum value represented by M_∞. This maximum value is equal to 1 divided by the dielectric constant at infinite frequency ($1/\varepsilon_\infty$). Relaxation phenomena become saturated at higher frequencies. At elevated values of M' (real part of complex modulus), the relaxation processes within the material become saturated. This means that the relaxation processes reach their maximum extent and cannot contribute further to changes in the behavior of the material at even higher frequencies. The relaxation processes are dispersed over a range of frequencies.

Fig. 4.12(a-f) depicts the variation of the imaginary component of modulus, M'', as a function of frequency at different temperatures for LiI concentrations ranging from $0\ to\ 25\ wt.\%$ in the LBP glass system. The plots depicting M'' vs $\log f$ exhibit a prolonged tail at lower frequencies, which can be attributed to the presence of significant capacitance associated with the electrodes. The spectral shape remains invariant; however, the frequency associated with the maximum modulus, M''_{max}, undergoes a shift towards higher frequency regions as the temperature increases. The spectra of M'' exhibit analogous behavior across all samples. The aforementioned facts suggest that the current glass systems can be regarded as feasible solid electrolytes that can be modelled using lumped R-C circuits (depicted in Fig. 4.3(g)). Comparable findings have been documented in other glasses that conduct ions [10], [43].

Fig. 4.13(a) describes the composition dependence of the M'' spectra (loss factor spectra) for an investigated system at a temperature of $373\ K$. The M'' spectra represent the imaginary part of the complex modulus, which is a measure of the energy dissipation or loss in a material. According to the observed trend, as the conductivity of the system increases due to the incorporation of LiI dopant salt, the maximum value of M''_{max} shifts towards higher frequencies.

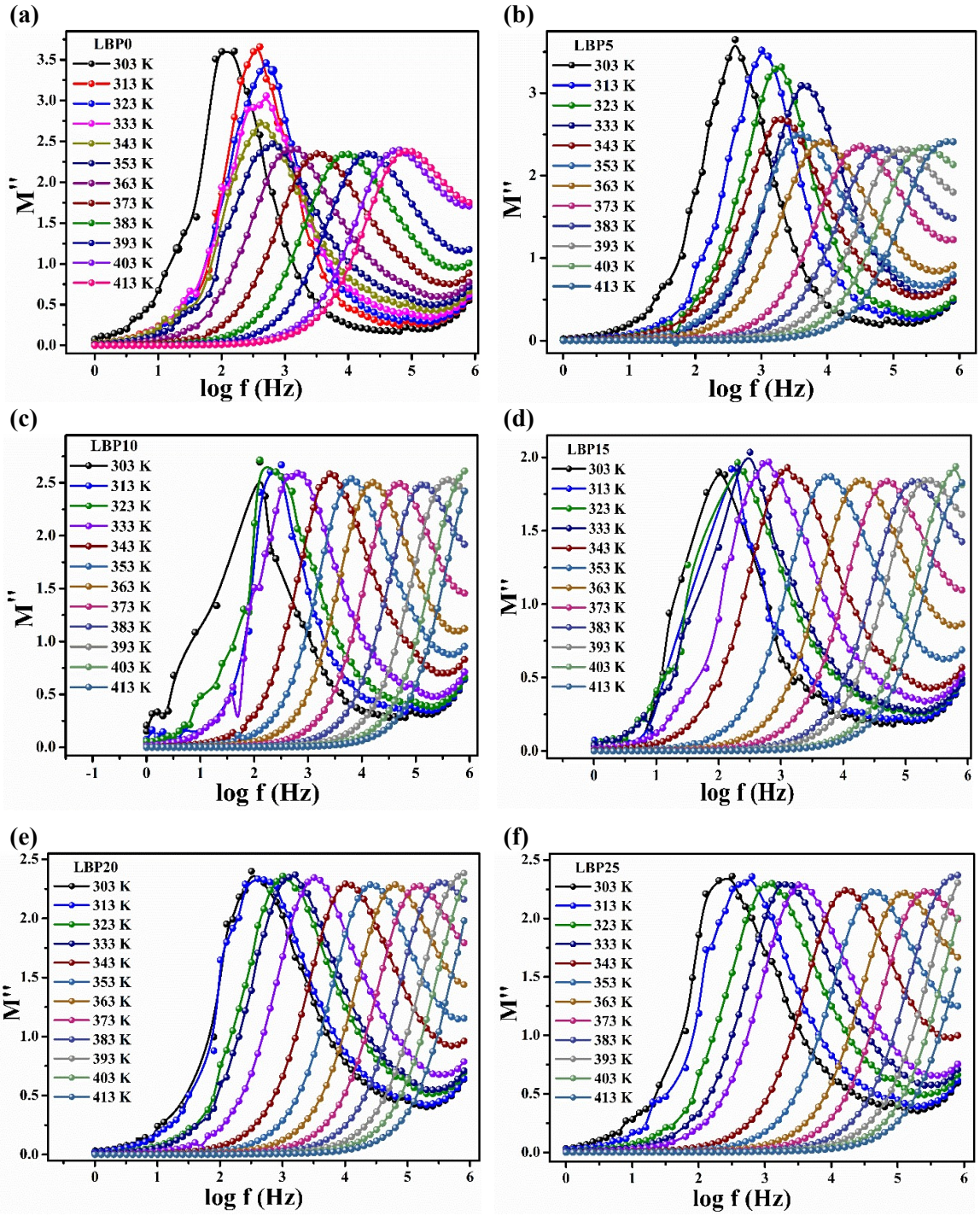

***Figure 4.12**:(a-f) The plot of $M''_{(\omega)}$as a function of frequency for xLiI addition in lithium borophosphate glass system, where $x = 0, 5, 10, 15, 20, 25\ wt.\%$ respectively.*

This suggests that the energy dissipation or loss in the material occurs at higher frequencies with increased conductivity. Additionally, the increase in dopant content is accompanied by a noticeable increase in the full width at half maxima (FWHM) for all LBP glass samples in the studied frequency range. The FWHM is a measure of the spectral bandwidth or spread of the energy dissipation peaks. Therefore, the broader FWHM indicates a broader range of

frequencies at which energy dissipation occurs. Furthermore, the statement mentions that many researchers have reported that the M''_{max} for all compositions is independent of temperature. This means that the position of the maximum value of M'' on the frequency axis remains constant with temperature variations. However, the researchers have also noted that the M''_{max} increases with an increase in the lithium salt content [10], [44], [45]. The model proposed by Macedo is capable of predicting the low and high frequency variations of M' and M''[46]. As per this model, M' and M'' exhibit a tendency towards zero means that when the product of angular frequency (ω) and the relaxation time (τ_σ) is significantly less than one ($\omega\tau_\sigma << 1$), both M' and M'' tend to approach zero. This behavior suggests that the system has a dominant capacitive response.

On the other hand, when $\omega\tau_\sigma$ is significantly less than one ($\omega\tau_\sigma << 1$), M' reaches the value of (M_s). This indicates that the system exhibits a dominant inductive response. The behavior described above is consistent with the model proposed by Macedo, and the observed outcomes in the current system align with the expectations based on the model. Regarding the frequency at which the maximum of M'' is observed, denoted by ω_C, its occurrence signifies the transition from short-range to long-range mobility as the frequency decreases. This transition is governed by the condition $\omega_C\tau_C = 1$, where τ_C represents the characteristic relaxation time associated with the transition. In summary, the occurrence of the maximum of M' at ω_C indicates the transition from short-range to long-range mobility, with the specific frequency governed by the condition $\omega_C\tau_C = 1$ [44], [47].

Fig. 4.13(b) illustrates the logarithmic relationship between τ_C (or $f_{max} = 1/\tau_C$), plotted against the reciprocal of temperature for various glass samples, in accordance with the concepts of Arrhenius law. The impedance spectrum (E_σ) is indicative of long-range charge transport, while the modulus spectrum (E_τ) provides insight into short-range migration through the activation energy. Our findings reveal that these two values are comparable in magnitude, as shown in Fig. 4.13(c), suggesting that lithium ion transport in the current system occurs via hopping mechanisms, regardless of whether the migration is long or short range [44].

The results suggest that as the amount of dopant salt increases, the full width at half maximum (FWHM) also increases. The FWHM values obtained for the LBP0 to LBP25 samples range from approximately 1.21 to 2.36 decades, respectively. It is worth noting that these values exceed the expected range of 1.14 decades for ideal Debye behavior. The deviation from the expected Debye behavior is often interpreted as an indication of the

distribution of relaxation times during the conduction mechanism. In other words, it suggests that the system exhibits a range of relaxation times rather than a single characteristic time. Furthermore, there is a known relationship between the distribution of relaxation times and the distribution of free energy barriers for ionic jumps. This relationship implies that variations in the energy barriers experienced by ions in the material contribute to the observed distribution of relaxation times. The distribution of relaxation times and the distribution of free energy barriers for ionic jumps are connected because the energy barriers influence the rates at which ions can transition between different states or positions. Variations in the energy barriers result in ions experiencing different relaxation times, leading to a broadened distribution.

In the context of the distribution of free energy barriers and the conduction process, different researchers have proposed different explanations. Hasz [48] suggests that the distribution of free energy barriers increases with increasing disorder in the system. On the other hand, Grant [49] argues that the distribution of free energy barriers reflects the cooperative nature of the conduction process. The Kohlrausch relaxation function, also known as the stretched exponential function, is attributed to the cooperative behavior of charge carriers in conductivity relaxation, as explained by Ngai and Martin [50]. This function describes the non-symmetric relaxation behavior often observed in complex systems. The non-symmetric modulus plot resulting from the behavior of the electrical function can be accurately described by the KWW (Kohlrausch-Williams-Watts) exponential function. This function incorporates the Kohlrausch exponent, denoted as β, and the conductivity relaxation parameter, denoted by τ. The Kohlrausch exponent, β, determines the shape of the relaxation function and describes the degree of asymmetry or stretched behavior.

A value of β closer to 1 indicates a more symmetric or exponential relaxation, while a smaller β value indicates a more stretched or non-exponential relaxation. The conductivity relaxation parameter, τ, represents the characteristic relaxation time associated with the conduction process. It influences the time scale at which the relaxation behavior occurs.

The current system, Fig. 4.13(d), has determined that the β is at its minimum value when a $25\ wt.\%$ addition of LiI is incorporated into the host lithium borophosphate glass. The function deviating from the linear exponential behavior suggests that the relaxation process in the system does not follow a simple exponential decay. The concept of collaborative movements within a glass, which describes the behavior of charge carriers, was initially proposed by Jonscher [68], [69].

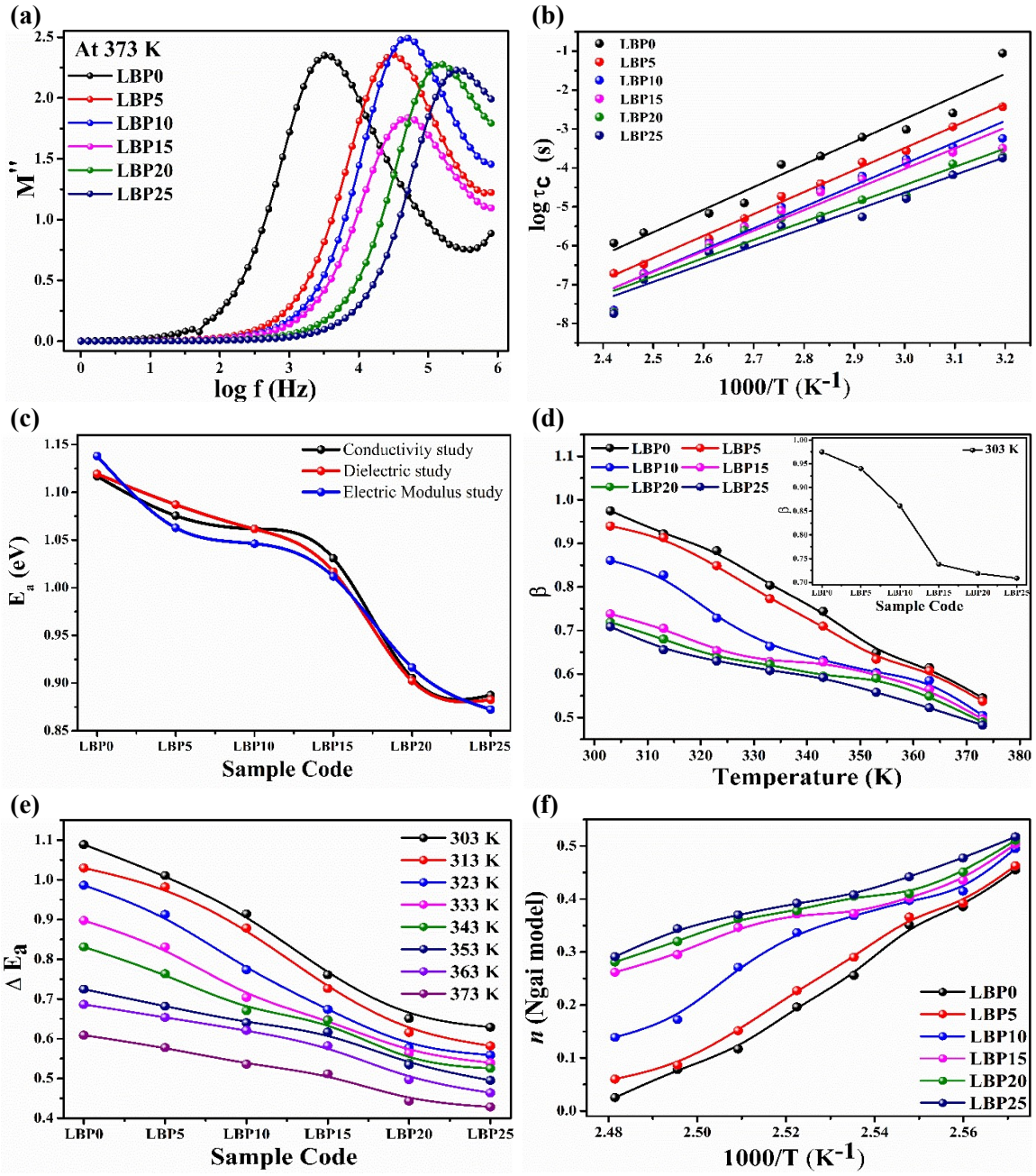

***Figure 4.13**:(a) At 373 K temperature, the plot of composition dependence $M''_{(\omega)}$ spectra., (b) Arrhenius behavior of modulus relaxation time, (c) Comparison of activation energy obtained from conductivity, dielectric and electric modulus study, (d) β, stretching parameter as a function of temperature, inset: room temperature trend of β for all samples, (e) Primitive activation energy according to Ngai model, for glass samples at various temperatures, and (f) coupling parameter as a function of reciprocal of temperature for all the series samples.*

According to this concept, the movement of a mobile ion within a glass cannot be considered an independent occurrence. When an ion transitions from one equilibrium state to another, it induces a temporary displacement of other charged particles in its vicinity. This displacement leads to additional relaxation of the external electric field. In other words, the movement of one charge carrier triggers cooperative effects that influence the behavior

of other charge carriers in the system. This cooperative behavior results in a non-linear relaxation process and is often characterized by a stretched exponential or non-exponential relaxation function. The stretching parameter β, which lies as $0 < \beta < 1$, is inversely proportional to the degree of charge carrier cooperation. A smaller value of β indicates a higher degree of cooperation among charge carriers, leading to a more stretched or non-exponential relaxation behavior [51]. This concept provides insights into the complex dynamics and cooperative behavior observed in glassy materials, contributing to our understanding of conductivity relaxation and the collective motion of charge carriers within these systems. Multiple research investigations have been conducted to examine the correlation between the β and ΔE_σ parameters and the alkali oxide content in oxide glasses. The findings of these studies indicate that the β and ΔE_σ values exhibit a simultaneous decrease with an increase in the concentration of alkali oxide, as reported by Martin et al; and Balzer et al; [52]–[54]. A comparable outcome has been achieved in the case of presently investigated oxide glasses, which pertains to the concentration of lithium salt in the oxide glass. Ngai has made a significant contribution by establishing a correlation between the activation energy (ΔE_σ) and the Kohlrausch exponent (β) for a substantial number of oxide glasses. This correlation aligns with the coupling model of relaxation. This finding is consistent with previous research conducted by Ingram [55] and Ngai [56].

In his work, Ngai (1989) introduced the concept of a "primitive" activation energy, denoted as ΔE_a, which is expressed as $(1-n)\,\Delta E_\sigma$. Here, ΔE_σ represents the activation energy associated with macroscopic conductivity, and n is the coupling parameter, where $n = 1 - \beta$ [50]. The coupling parameter n is derived from the Kohlrausch exponent β. The primitive activation energy, ΔE_a, represents the energy barrier experienced by the population of mobile ions. This barrier arises from two main factors: The Coulombic forces acting on the charged ion and the strain force resulting from volume constraints in the conduction transition state between sites. This description of the energy barrier is supported by the Anderson-Stuart model [57].

The coupling model of relaxation suggests that the degree of cooperation among charge carriers, as indicated by the Kohlrausch exponent β, is related to the activation energy (ΔE_σ) and the primitive activation energy (ΔE_a). The correlation established by Ngai between ΔE_σ and β further supports the connection between the energy barriers experienced by charge carriers and their cooperative behavior in relaxation processes. Overall, these concepts contribute to our understanding of the relationship between activation energy, the

Kohlrausch exponent, and the cooperative dynamics of charge carriers in oxide glasses. They provide insights into the mechanisms underlying the relaxation processes in these materials.

The primitive activation energy at various temperatures for different glass samples is presented in Fig. 4.13(e). In this study, the coupling parameter (n) is introduced as a model parameter that characterizes the degree of non-exponential behavior and the extent to which mobile ions are linked during conduction. The findings of the study are consistent with previous research [50], which suggests that the research focuses on studying the correlation between the activation enthalpy and the Kohlrausch exponent for ionic conductivity in alkali alumino-germanate glasses. The activation enthalpy represents the energy barrier that needs to be overcome for ion migration. The Kohlrausch exponent is a parameter that describes the shape of the relaxation process in the conductivity of a material. As the concentration of mobile ions increases, the coupling between charge carriers becomes more pronounced. This increased coupling leads to a relaxation process that follows a stretched exponential distribution with β value less than unity, as illustrated in Fig. 4.13(f). It is important to note that the β value and the ΔE_σ parameters are determined experimentally and independently from each other. This implies that the non-exponential behavior of relaxation observed in the study is influenced by factors other than just the activation energy. Fig. 4.14(a) depicts the variation of β as a function of ΔE_σ for the investigated Li^+ ion conducting glass.

It can be described that the characteristic curve of a system, which exhibits two distinct domains. The first region corresponds to values of ΔE_σ (activation enthalpy) ranging from $0.88\ eV$ to $1.02\ eV$. In this region, regardless of the specific ΔE_σ value, the β value (Kohlrausch exponent) remains constant. In the second region, characterized by high ΔE_σ values $(> 1.02\ eV)$, the β value increases rapidly as ΔE_σ increases. This indicates that there is a lack of linear correlation between ΔE_σ and the degree of non-exponentially (as represented by the β value). In the first region, the β value does not change significantly as the activation enthalpy varies. However, in the second region with higher activation enthalpies, the β value increases rapidly. This suggests that the relationship between the activation enthalpy ΔE_σ) and the degree of non-exponentiality (as indicated by the β value) is not a simple linear correlation. Fig. 4.14(b) illustrates the relationship between the beta parameter and the average distance between $Li^+ - Li^+$ in Li^+ ion conducting LBP glass.

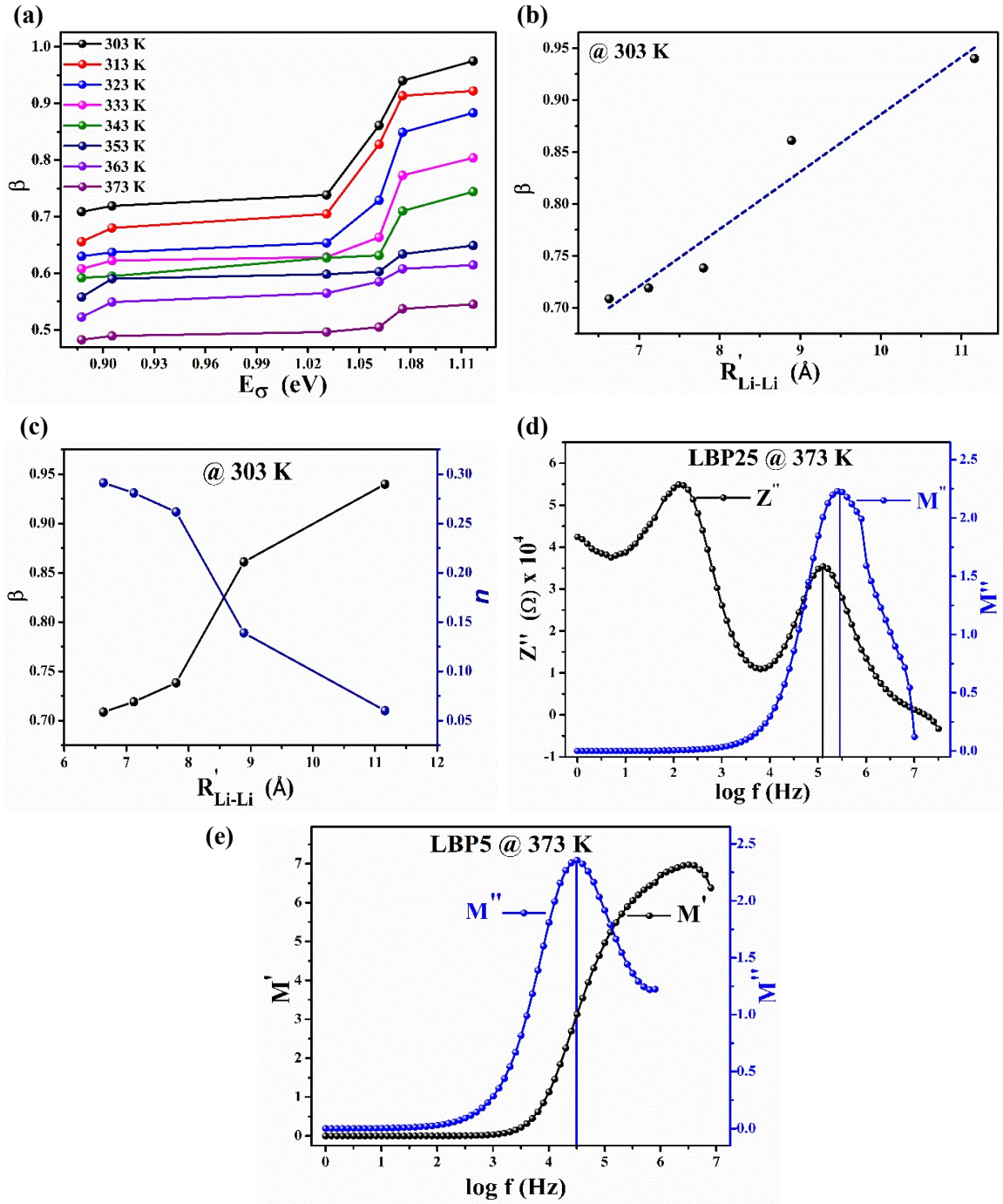

***Figure 4.14**: (a) Stretching parameter as a function of macroscopic conduction activation energy, (b) KWW component as a function of average distance between Li $^{+}$ions at room temperature, (c) Both stretching and coupling parameters as a function of average distance between cations, (d-e) for LBP25 sample and at 373K temperature, imaginary part of impedance and modulus and real and imaginary part of modulus as a function of frequency, respectively.*

The experimentally obtained data are observed to be distributed on either side of a dotted line. This observation indicates that the β parameter in the Kohlrausch relaxation function exhibits a strong correlation with the separation distance between Li^{+} ions in the Li^{+} borophosphate glass under consideration. This finding provides compelling evidence in

support of the hypothesis that the conductivity dispersion in frequency is a result of ion-ion coupling [58]. Fig. 4.14(c) explains the variation of beta parameter and the $n(T)$ as a function of R'_{Li-Li}. It can be described that the impedance and modulus spectra presented in Fig. 4.14(d) in order to understand the non-Debye characteristics of the current glass system. The occurrence of Z''_{max} (imaginary part of impedance) and M''_{max} (imaginary part of modulus) at different frequencies indicates the presence of a broad distribution of relaxation times within the system. This suggests that there is not a single dominant relaxation process, but rather multiple relaxation processes occurring simultaneously.

West et al; [59] suggested that previous research has established that the expansion of the M'' spectra at higher frequencies is associated with the presence of a distribution of relaxation times. This expansion indicates that there are different relaxation processes happening at different time scales within the system. On the other hand, the significant amplification in the broadening of the Z'' spectra at lower frequencies is attributed mainly to electrode polarization. Electrode polarization occurs when there is a buildup of charge at the electrode-electrolyte interface, leading to deviations in the electrical response of the system at low frequencies. Notably, from Fig. 4.14 (e),the relaxation peak of the imaginary component of the modulus aligns with the corresponding dispersion region of the real part of the modulus spectra for 5 $wt.\%$ addition of LiI in the host glass at 373 K temperature.

Modulus Scaling

The passage explains the formalization of modulus measurement, which involves assessing both the real (M') and imaginary (M'') components. The M'' component specifically reflects the dissipation of energy within the material, providing information about the relaxation processes occurring in the material. The M'' spectrum is found to be independent of temperature, indicating that the ionic mechanism responsible for relaxation is not influenced by temperature variations. This phenomenon is known as time-temperature superposition (TTS). TTS allows for the superimposition of relaxation processes occurring at different temperatures onto a single master curve by appropriately scaling the spectra.
The influence of glass composition on the shape of the M'' spectrum is highlighted as noteworthy. It is observed that the width of the M'' spectrum increases with a higher concentration of ions in the glass. This observation suggests that the overall concentration of mobile ions in the glass has an impact on the relaxation mechanism.

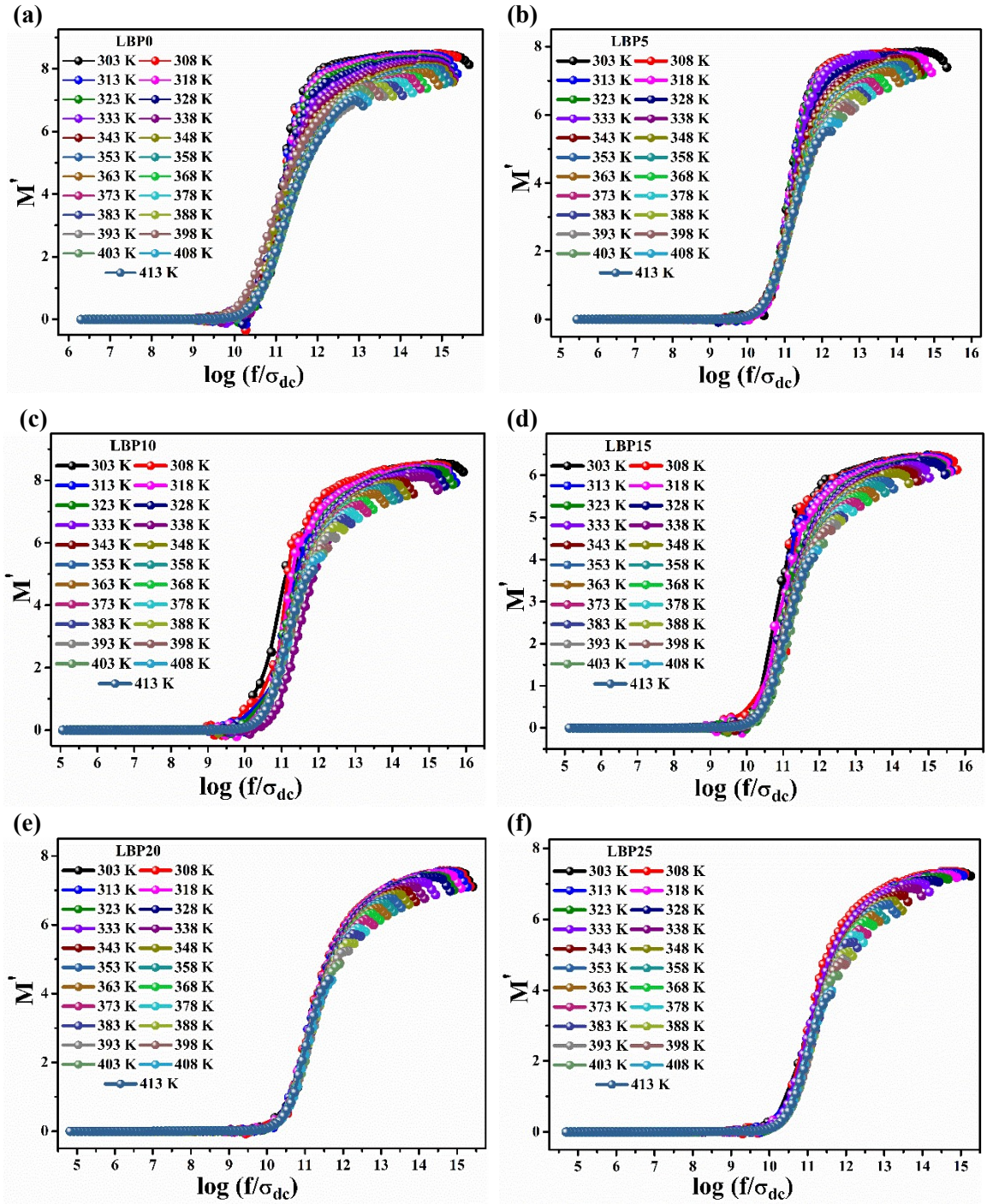

Figure 4.15: (a-f) *Normalized plots of the real part of the modulus (M') as a function of scaled frequency using Taylor-Isard-Scaling (T-I-S) formalism for all the series samples.*

The implication of this statement is that by modifying the concentration of mobile ions in the glass through compositional changes, the relaxation behavior and energy dissipation within the material can be adjusted. This finding highlights the importance of considering the composition of the glass when studying and designing materials with desired relaxation properties.

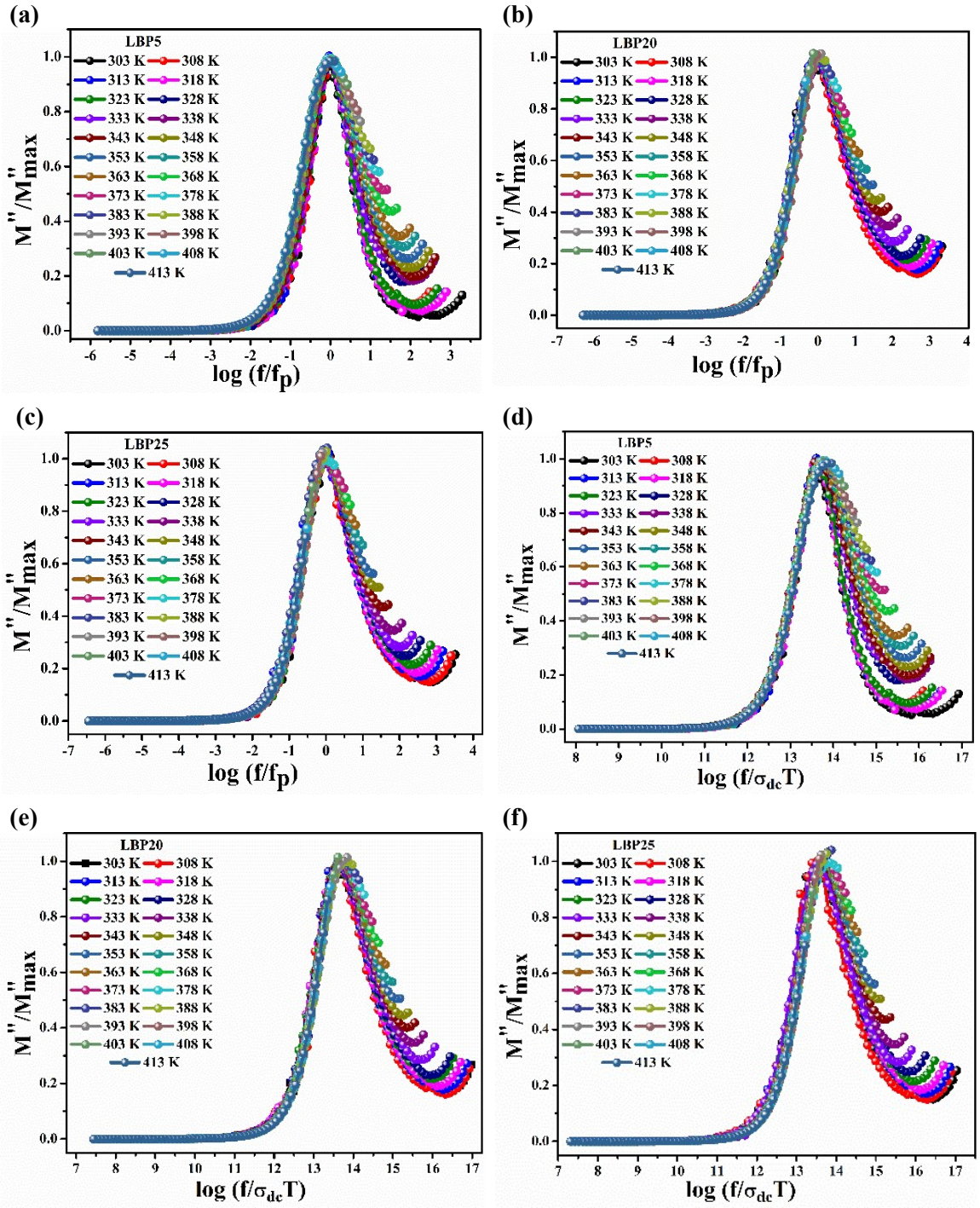

***Figure 4.16**: At various temperature, normalized plots of the imaginary part of the modulus (M'') as a function of scaled frequency using (a-c) Ghosh formalism and (d-f) Roling formalism, for all the series samples.*

The utilization of the Taylor-Isard-Scaling (T-I-S) formalism [60], [61] in the current glass system to scale the real component of modulus has been used. This is achieved by applying the function f/σ_{dc}, where f represents the frequency and σ_{dc} denotes the direct current (dc) conductivity. This scaling allows for the comparison of the real component of modulus at different frequencies while taking into account the conductivity of the system.

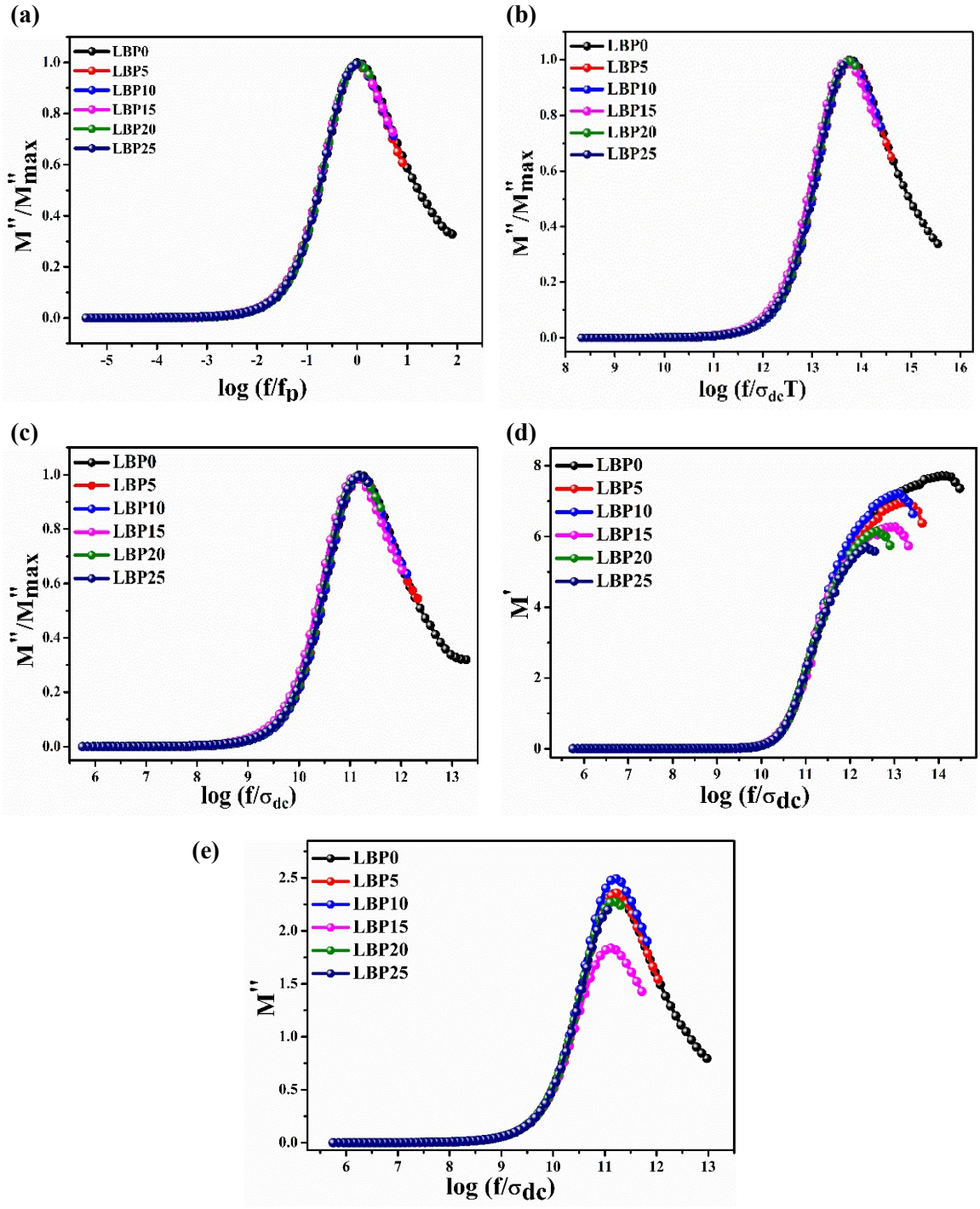

***Figure 4.17**: For all the glass compositions, the normalized frequency of imaginary part of the modulus as a function of scaled frequency using (a) Ghosh, (b) Roling and (c) Isard formalisms, (d-e) the real and imaginary part of modulus formalism as a function of scaled frequency according to T-I-S formulation, respectively.*

Furthermore, the $M^{"}$ spectrum is scaled using the Roling formalism [62], [63]. This formalism involves utilizing $M^{"}_{max}$ (the maximum value of the imaginary component of modulus) and its corresponding maximum frequency, f_{max}. The scaling of $M^{"}$ with respect

to frequency is performed using either the Ghosh model, with $\log(f/f_p)$ as the scaling parameter, or the Roling model, with $\log(f/\sigma_{dc}\,T)$ as the scaling parameter.

Fig. 4.15(a-f) displays the scaling of M' vs $\log(f/\sigma_{dc})$, showing the relationship between the real component of modulus and the scaled frequency. Fig. 4.16(a-c) illustrates the scaling of M''/M''_{max} with $\log(f/f_p)$ (Ghosh model), while Fig. 4.16(d-f) demonstrate the scaling with $\log(f/\sigma_{dc}\,T)$ (Roling model). These figures present the results of the scaling analysis at different temperatures for all glass compositions.

The presence of curves across various temperatures implies that the dynamic phenomenon occurring at distinct frequencies remains unaffected by changes in temperature. Moreover, it has been discovered that the M' and M''spectra obtained at varying temperatures can be consolidated into a unified master curve through the corresponding utilization of T-I-S and Roling scaling formulations. The curve obtained indicates that various dynamic processes taking place at distinct time scales exhibited identical activation energy and that the temperature-independent relaxation time distribution was present. The Ghosh formalism illustrates that the normalized modulus function, M''/M''_{max}, exhibits a singular master curve when logarithmically scaled with $\log(f/f_p)$, as shown in Fig. 4.17(a-c).

Several scaling formalisms [36], [37], [61], [64], [65] were employed in multiple attempts and the resultant curves are integrated into a single master curve.

However, Fig. 4.17(d-e), the real and/or imaginary component of the modulus failed to converge into a singular master curve. This was particularly evident in the dispersive frequency region, suggesting that the relaxation mechanism is influenced by the glass compositions. The suggestion is made that various dynamic processes occurring at distinct time scales demonstrate identical activation energy and that the dispersed relaxation time remains unaffected by temperature.

4.4 Conclusion

It can be attributed that the $[60Li_2O:(8\,B_2O_3 + 32\,P_2O_5)]$ glass system upon the addition of lithium iodide (LiI) transforms the glass into an ionic conductor, where the Li^+ ions dissociate from LiI that hop and conduct within the glass structure according to the Correlated Barrier Hopping (CBH) model. The addition of LiI leads to an increased openness of the glass structure, without major structural modifications or significant

changes in the glass transition temperature. The depolymerization of the phosphate chain network and polymerization of the borate chain network are observed, resulting in the transformation from ring-type structures of BO_3 units to BO_4 units in the glass. This structural change facilitates the transport of Li^+ ions by opening up the glass network. The conductivity of the glass samples follows the Jonscher power law, indicating a frequency-dependent conductivity. The variation of the parameter $n(T)$, obtained experimentally, and the calculated theoretical values of $n(T)$ using R_{min} and U_M values, show the same trend.

- This suggests that in the present glass system, the transport of Li^+ ions occur through the *Correlated Barrier Hopping* (CBH) mechanism. Furthermore, the conductivity and modulus functions have been scaled using various formalisms proposed by *Ghosh, Roling, Summerfield, and Taylor-Isard*. These scaling formalisms likely allow for a better understanding of the frequency and temperature dependence of the conductivity and modulus properties in the glass system.

In addition to that, the study highlights several important findings regarding the Li^+ ion migration and conductivity relaxation in lithium borophosphate glasses doped with LiI.

- First, the activation energy obtained from both impedance and modulus spectra is very close, indicating that the migration of Li^+ ions in the glass occurs through a hopping mechanism. This suggests that the ions move by jumping from one location to another within the glass structure. The relaxation of conductivity in the glass system is well described by the Kohlrausch-Williams-Watts (KWW) function, which is a stretched exponential function commonly used to describe relaxation processes.
- The Coupling model proposed by Ngai is employed to analyze the variation of the stretching parameter (β) and the coupling parameter (n) with the LiI content in the glass. The results confirm the validity of this model for describing the conduction of Li^+ ions in lithium borophosphate glasses.
- The variation of β and $n(T)$ indicates a strong ion-ion coupling between the charge carriers and a significant decoupling between the Li^+ ion conducting motions and the viscous motions of the glass framework. This suggests that the conductivity enhancement in borophosphate glasses with high LiI content is associated with both increased ion-ion coupling and reduced coupling between the Li^+ ions and the glass matrix.

Overall, these findings provide insights into the conduction mechanism and behavior of lithium borophosphate glasses doped with LiI, emphasizing the importance of ion-ion coupling and the influence of *LiI* content on the conductivity and relaxation properties of the glass system.

Bibliography

[1] V. A. Adhwaryu and D. K. Kanchan, "Effect of Lithium Iodide on transport phenomenon in Lithium Borophosphate glass Electrolyte," J. Non. Cryst. Solids, vol. 583, p. 121474, May 2022, doi: 10.1016/J.JNONCRYSOL.2022.121474.

[2] N. KARAN, B. NATESAN, and R. KATIYAR, "Structural and lithium ion transport studies in borophosphate glasses," Solid State Ionics, vol. 177, no. 17–18, pp. 1429–1436, Jul. 2006, doi: 10.1016/j.ssi.2006.07.032.

[3] A. R. Kulkarni, H. S. Maiti, and A. Paul, "Fast ion conducting lithium glasses-Review," Bull. Mater. Sci., vol. 6, no. 2, pp. 201–221, 1984, doi: 10.1007/BF02743897.

[4] H. Wada, M. Menetrier, A. Levasseur, and P. Hagenmuller, "Preparation and ionic conductivity of new B2S3-Li2S-LiI glasses," Mater. Res. Bull., vol. 18, no. 2, pp. 189–193, 1983, doi: 10.1016/0025-5408(83)90080-6.

[5] D. D. Ramteke and R. S. Gedam, "Study of Li2O-B2O3-Dy2O 3 glasses by impedance spectroscopy," Solid State Ionics, vol. 258, pp. 82–87, May 2014, doi: 10.1016/j.ssi.2014.02.006.

[6] D. D. Ramteke, H. C. Swart, and R. S. Gedam, "Electrochemical response of Nd 3+ ions containing lithium borate glasses," J. Rare Earths, vol. 35, no. 5, pp. 480–484, May 2017, doi: 10.1016/S1002-0721(17)60937-2.

[7] J. Mizerakova, P. Hockicko, and F. Munoz, "Dielectric Study of Lithium and Sodium Borophosphate Glasses," Commun. - Sci. Lett. Univ. Zilina, vol. 19, no. 3, pp. 46–50, Sep. 2017, doi: 10.26552/com.C.2017.3.46-50.

[8] D. Larink, H. Eckert, M. Reichert, and S. W. Martin, "Mixed network former effect in ion-conducting alkali borophosphate glasses: Structure/property correlations in the system [M2O] 1/3[(B2O3)x(P2O 5)1- X]2/3 (M = Li, K, Cs)," J. Phys. Chem. C, vol. 116, no. 50, 2012, doi: 10.1021/jp307085t.

[9] F. S. Howell, R. A. Bose, P. B. Macedo, and C. T. Moynihan, "Electrical Relaxation in a Glass-Forming Molten Salt."

[10] V. A. Adhwaryu and D. K. Kanchan, "Ag+ ion conduction in AgI-Ag2O-B2O3-P2O5 glass electrolyte," Mater. Sci. Eng. B Solid-State Mater. Adv. Technol., vol. 263, 2021, doi: 10.1016/j.mseb.2020.114857.

[11] D. Toloman et al., "Phosphate Glassy Network Depolymerization Induced by CaO Doping,"

Part. Sci. Technol., vol. 28, no. 3, pp. 226–235, May 2010, doi: 10.1080/02726351.2010.481581.

[12] B. N. Nelson and G. J. Exarhos, "Vibrational spectroscopy of cation-site interactions in phosphate glasses," J. Chem. Phys., vol. 71, no. 7, p. 2739, 1979, doi: 10.1063/1.438679.

[13] A. M. Efimov, "IR fundamental spectra and structure of pyrophosphate glasses along the 2ZnO · P2O5-2Me2O · P2O5 join (Me being Na and Li)," J. Non. Cryst. Solids, vol. 209, no. 3, pp. 209–226, 1997, doi: 10.1016/S0022-3093(96)00562-5.

[14] M. Taylor, R. Norbury, S. Murphy, S. Rudebeck, P. Jezzard, and P. Cowen, "Lack of effect of citalopram on magnetic resonance spectroscopy measures of glutamate and glutamine in frontal cortex of healthy volunteers," J. Psychopharmacol., vol. 24, no. 8, pp. 1217–1221, Aug. 2010, doi: 10.1177/0269881109105679.

[15] M. Htut, M. Lwin, P. Kaung, and S. Htoon, No Title, vol. IV, no. 2. 2006. [Online]. Available: http://www.iaea.org/inis/collection/NCLCollectionStore/_Public/40/057/40057374.pdf

[16] T. Q. & M. Leow, T. & I. Leong & Eeu, Zuhairi & Hussin, and Rosli, "Study of Structural and Luminescence Properties of Lead Lithium Borophosphate Glass System Doped with Ti Ions. Sains Malaysiana. 43. 929-934. ," Sains Malaysiana. , vol. 43., pp. 929-934., 2014.

[17] El-Batal et al., "Optical and infrared properties of lithium diborate glasses doped with copper oxide: Effect of gamma irradiation," Indian J. Pure Appl. Phys., vol. 50(06), Jun. 2012.

[18] S. Kabi and A. Ghosh, "Mixed glass former effect in AgI doped silver borophosphate glasses," Solid State Ionics, vol. 262, pp. 778–781, Sep. 2014, doi: 10.1016/j.ssi.2013.09.028.

[19] Y. M. Lai, X. F. Liang, S. Y. Yang, J. X. Wang, L. H. Cao, and B. Dai, "Raman and FTIR spectra of iron phosphate glasses containing cerium," J. Mol. Struct., vol. 992, no. 1–3, pp. 84–88, Apr. 2011, doi: 10.1016/j.molstruc.2011.02.049.

[20] N. J. Kim, S. H. Im, D. H. Kim, D. K. Yoon, and B. K. Ryu, "Structure and properties of borophosphate glasses," Electron. Mater. Lett., vol. 6, no. 3, pp. 103–106, Sep. 2010, doi: 10.3365/eml.2010.09.103.

[21] W. M. Hua, P. S. Wong, R. Hussin, and Z. Ibrahim, "Structural Study on Lithium-Barium Borophosphate Glasses Using Infrared and Raman Spectroscopy," Adv. Mater. Res., vol. 626, pp. 11–15, Dec. 2012, doi: 10.4028/www.scientific.net/AMR.626.11.

[22] C. Gautam, A. K. Yadav, and A. K. Singh, "A Review on Infrared Spectroscopy of Borate Glasses with Effects of Different Additives," ISRN Ceram., vol. 2012, pp. 1–17, 2012, doi: 10.5402/2012/428497.

[23] H. A. Othman, H. S. Elkholy, and I. Z. Hager, "FTIR of binary lead borate glass: Structural investigation," J. Mol. Struct., vol. 1106, pp. 286–290, Feb. 2016, doi: 10.1016/j.molstruc.2015.10.076.

[24] V. N. Rai, B. N. Raja Sekhar, D. M. Phase, and S. K. Deb, "EFFECT OF GAMMA IRRADIATION ON THE STRUCTURE AND VALENCE STATE OF Nd IN PHOSPHATE GLASS."

[25] J. F. Ducel and J. J. Videau, "Physical and chemical characterizations of sodium borophosphate glasses," Mater. Lett., vol. 13, no. 4–5, pp. 271–274, Apr. 1992, doi: 10.1016/0167-577X(92)90230-H.

[26] A. H. Ahmad and A. K. Arof, "Structural studies and ionic conductivity of lithium iodide-lithium tungstate solid electrolytes," Ionics (Kiel)., vol. 8, no. 5–6, pp. 433–438, Sep. 2002, doi: 10.1007/BF02376058.

[27] L. Balachander, G. Ramadevudu, M. Shareefuddin, R. Sayanna, and Y. C. Venudharc, "IR analysis of borate glasses containing three alkali oxides," ScienceAsia, vol. 39, no. 3, pp. 278–283, Jun. 2013, doi: 10.2306/scienceasia1513-1874.2013.39.278.

[28] Y. M. Moustafa and K. El-Egili, "Infrared spectra of sodium phosphate glasses," J. Non. Cryst. Solids, vol. 240, no. 1–3, 1998, doi: 10.1016/S0022-3093(98)00711-X.

[29] D. Carta et al., "The effect of composition on the structure of sodium borophosphate glasses," J. Non. Cryst. Solids, vol. 354, no. 31, pp. 3671–3677, Aug. 2008, doi: 10.1016/J.JNONCRYSOL.2008.04.009.

[30] J. J. Hudgens and S. W. Martin, Mid-IR and far-IR investigation of AgI-doped silver diborate glasses, vol. 53, no. 9. 1996, pp. 5348–5355. doi: 10.1103/PhysRevB.53.5348.

[31] A. Moguš-Milanković et al., "Electrical, dielectric and spectroscopic studies on MnO doped LiI-AgI-B 2O 3 glasses," J. Appl. Phys., vol. 111, no. 1, pp. 0–11, 2012, doi: 10.1063/1.3676254.

[32] N. Satyanarayana, A. Karthikeyan, and M. Venkateswarlu, "A.c. conductivity studies on the silver molybdo-arsenate glassy system," J. Mater. Sci., vol. 31, no. 20, pp. 5471–5477, 1996, doi: 10.1007/BF01159319.

[33] M. Dult, R. S. Kundu, S. Murugavel, R. Punia, and N. Kishore, "Conduction mechanism in bismuth silicate glasses containing titanium," Phys. B Condens. Matter, vol. 452, pp. 102–107, Nov. 2014, doi: 10.1016/j.physb.2014.07.004.

[34] K. H. Mahmoud, F. M. Abdel-Rahim, K. Atef, and Y. B. Saddeek, "Dielectric dispersion in lithium–bismuth-borate glasses," Curr. Appl. Phys., vol. 11, no. 1, pp. 55–60, Jan. 2011, doi: 10.1016/j.cap.2010.06.018.

[35] A. K. Jonscher, "Analysis of the alternating current properties of ionic conductors," J. Mater. Sci., vol. 13, no. 3, pp. 553–562, Mar. 1978, doi: 10.1007/BF00541805.

[36] S. Summerfield, "Universal low-frequency behaviour in the a.c. hopping conductivity of disordered systems," Philos. Mag. B Phys. Condens. Matter; Stat. Mech. Electron. Opt. Magn. Prop., vol. 52, no. 1, pp. 9–22, 1985, doi: 10.1080/13642818508243162.

[37] B. Roling, A. Happe, K. Funke, and M. D. Ingram, No Title, vol. 78, no. 11. 1997, pp. 2160–

2163. doi: 10.1103/PhysRevLett.78.2160.

[38] B. Roling, A. Happe, K. Funke, and M. D. Ingram, "Carrier Concentrations and Relaxation Spectroscopy: New Information from Scaling Properties of Conductivity Spectra in Ionically Conducting Glasses," Phys. Rev. Lett., vol. 78, no. 11, pp. 2160–2163, Mar. 1997, doi: 10.1103/PhysRevLett.78.2160.

[39] A. Radoń, D. Łukowiec, M. Kremzer, J. Mikuła, and P. Włodarczyk, "Electrical conduction mechanism and dielectric properties of spherical shaped Fe3O4 nanoparticles synthesized by co-precipitation method," Materials (Basel)., vol. 11, no. 5, p. 735, May 2018, doi: 10.3390/ma11050735.

[40] H. Darwish and M. M. Gomaa, "Effect of compositional changes on the structure and properties of alkali-alumino borosilicate glasses," J. Mater. Sci. Mater. Electron., vol. 17, no. 1, pp. 35–42, Jan. 2006, doi: 10.1007/s10854-005-5139-2.

[41] M. S. Jayswal, D. K. Kanchan, P. Sharma, and N. Gondaliya, "Relaxation process in PbI2-Ag2O-V2O 5-B2O3 system: Dielectric, AC conductivity and modulus studies," Mater. Sci. Eng. B Solid-State Mater. Adv. Technol., vol. 178, no. 11, pp. 775–784, Jun. 2013, doi: 10.1016/j.mseb.2013.03.013.

[42] D. K. Kanchan, K. P. Padmasree, H. R. Panchal, and A. R. Kulkarni, "Electrical transport studies on CdI2 doped silver oxysalt system," Ceram. Int., vol. 30, no. 7, pp. 1655–1660, Jan. 2004, doi: 10.1016/j.ceramint.2003.12.160.

[43] B. CHOWDARI and R. GOPALAKRISHNAN, "Impedance and modulus spectroscopy of vitreous AgI□Ag2O□P2O5 system," Solid State Ionics, vol. 18–19, pp. 483–487, Jan. 1986, doi: 10.1016/0167-2738(86)90164-5.

[44] B. CHOWDARI and R. GOPALAKRISHNAN, "ac conductivity analysis of glassy silver iodomolybdate system☆," Solid State Ionics, vol. 23, no. 3, pp. 225–233, Apr. 1987, doi: 10.1016/0167-2738(87)90055-5.

[45] P. Sharma, D. K. Kanchan, M. Pant, N. Gondaliya, and M. S. Jayswal, "Study of relaxation dynamics in mixed iodide doped silver-vanado-borate superionic glass system," in AIP Conference Proceedings, 2011, vol. 1349, no. PART A. doi: 10.1063/1.3605977.

[46] P. B. Macedo, C. T. Moynihan, and R. Bose, "The Role of Ionic Diffusion in Polarization in Vitreous Ionic.," Phys. Chem. Glas., vol. 13, no. 6, pp. 171–179, 1972.

[47] M. Sural and A. Ghosh, "Conductivity relaxation in zirconium fluoride glasses: effect of substitution of Zr4+ by Y3+ ions," Solid State Ionics, vol. 120, no. 1–4, pp. 27–32, May 1999, doi: 10.1016/S0167-2738(98)00551-7.

[48] W. . Hasz, C. . Moynihan, and P. . Tick, "Electrical relaxation in a CdF2□LiF□AlF3□PbF2 glass and melt," J. Non. Cryst. Solids, vol. 172–174, pp. 1363–1372, Sep. 1994, doi: 10.1016/0022-3093(94)90664-5.

[49] R. J. Grant, M. D. Ingram, L. D. S. Turner, and C. A. Vincent, "Optimized ionic conductivity in glass. Vitreous silver arsenate iodide (Ag7I4AsO4) electrolytes," J. Phys. Chem., vol. 82, no. 26, pp. 2838–2844, Dec. 1978, doi: 10.1021/j100515a019.

[50] K. L. Ngai, J. N. Mundy, H. Jain, O. Kanert, and G. Balzer-Jollenbeck, "Correlation between the activation enthalpy and Kohlrausch exponent for ionic conductivity in alkali aluminogermanate glasses," Phys. Rev. B, vol. 39, no. 9, pp. 6169–6179, Mar. 1989, doi: 10.1103/PhysRevB.39.6169.

[51] H. Jain, "Ion movement relaxation in inorganic glasses — salient features," J. Non. Cryst. Solids, vol. 131–133, pp. 961–968, Jun. 1991, doi: 10.1016/0022-3093(91)90709-F.

[52] S. W. Martin and C. A. Angell, "Dc and ac conductivity in wide composition range Li2OP2O5 glasses," J. Non. Cryst. Solids, vol. 83, no. 1–2, 1986, doi: σ_(523-623)≈〖10〗^(-8)-〖10〗^(-3).

[53] G. Balzer-Jöllenbeck, O. Kanert, H. Jain, and K. L. Ngai, "New interpretation of activation enthalpies for electrical conductivity and nuclear spin relaxation in glassy ionic conductors," Phys. Rev. B, vol. 39, no. 9, pp. 6071–6075, Mar. 1989, doi: 10.1103/PhysRevB.39.6071.

[54] S. W. Martin, "Conductivity relaxation in glass: Compositional contributions to non-exponentiality," Appl. Phys. A Solids Surfaces, vol. 49, no. 3, pp. 239–247, Sep. 1989, doi: 10.1007/BF00616850.

[55] M. D. Ingram, "Ionic Conductivity in Glass," Phys. Chem. Glas., pp. 214–234, 1987.

[56] K. L. Ngai and O. Kanert, No Title, vol. 53–56, no. PART 2. 1992, pp. 936–946. doi: 10.1016/0167-2738(92)90275-T.

[57] O. L. ANDERSON and D. A. STUART, "Calculation of Activation Energy of Ionic Conductivity in Silica Glasses by Classical Methods," J. Am. Ceram. Soc., vol. 37, no. 12, pp. 573–580, Dec. 1954, doi: 10.1111/j.1151-2916.1954.tb13991.x.

[58] J. REAU et al., "Conductivity relaxation parameters of some Ag+ conducting tellurite glasses containing AgI or the (AgI)0.75 (T1I)0.25 eutectic mixture," Solid State Ionics, vol. 74, no. 1–2, pp. 65–73, Dec. 1994, doi: 10.1016/0167-2738(94)90438-3.

[59] A. R. WEST, D. C. SINCLAIR, and N. HIROSE, "Characterization of Electrical Materials, Especially Ferroelectrics, by Impedance Spectroscopy," J. Electroceramics, vol. 1, no. 1, pp. 65–71, 1997, doi: 10.1023/A:1009950415758.

[60] J. C. Dyre, Universal low-temperature ac conductivity of macroscopically disordered nonmetals, vol. 48, no. 17. 1993, pp. 12511–12526. doi: 10.1103/PhysRevB.48.12511.

[61] J. O. Isard, "A study of the migration loss in glass and a generalized method of calculating the rise of dielectric loss with temperature," Proc. IEE - Part B Electron. Commun. Eng., vol. 109, no. 22S, pp. 440–447, 1962, doi: 10.1049/pi-b-2.1962.0077.

[62] T. B. Schrøder and J. C. Dyre, "Scaling and universality of ac conduction in disordered

solids," Phys. Rev. Lett., vol. 84, no. 2, pp. 310–313, 2000, doi: 10.1103/PhysRevLett.84.310.

[63] B. Roling, What do electrical conductivity and electrical modulus spectra tell us about the mechanisms of ion transport processes in melts, glasses, and crystals?, vol. 244, no. 1. Elsevier, 1999, pp. 34–43. doi: 10.1016/S0022-3093(98)00847-3.

[64] A. Ghosh and A. Pan, *Scaling of the conductivity spectra in ionic glasses: Dependence on the structure*, vol. 84, no. 10. 2000, pp. 2188–2190. doi: 10.1103/PhysRevLett.84.2188.

[65] A. Pan and A. Ghosh, *Relaxation dynamics of lithium ions in lead bismuthate glasses*, vol. 62, no. 5. 2000, pp. 3190–3195. doi: 10.1103/PhysRevB.62.3190.